Science Arts & Métiers (SAM)

is an open access repository that collects the work of Arts et Métiers Institute of Technology researchers and makes it freely available over the web where possible.

This is an author-deposited version published in: https://sam.ensam.eu
Handle ID: .http://hdl.handle.net/10985/14296

To cite this version :

El-Hadi TIKARROUCHINE, George CHATZIGEORGIOU, Yves CHEMISKY, Fodil MERAGHNI - Fully coupled thermo-viscoplastic analysis of composite structures by means of multi-scale three-dimensional finite element computations - International Journal of Solids and Structures p.in press - 2019

Any correspondence concerning this service should be sent to the repository Administrator : scienceouverte@ensam.eu

Arts et Métiers Institute of Technology

Accepted Manuscript

Fully coupled thermo-viscoplastic analysis of composite structures by means of multi-scale three-dimensional finite element computations

E. Tikarrouchine, G. Chatzigeorgiou, Y. Chemisky, F. Meraghni

PII: S0020-7683(19)30027-7
DOI: https://doi.org/10.1016/j.ijsolstr.2019.01.018
Reference: SAS 10249

To appear in: *International Journal of Solids and Structures*

Received date: 29 September 2018
Revised date: 20 December 2018
Accepted date: 12 January 2019

Please cite this article as: E. Tikarrouchine, G. Chatzigeorgiou, Y. Chemisky, F. Meraghni, Fully coupled thermo-viscoplastic analysis of composite structures by means of multi-scale three-dimensional finite element computations, *International Journal of Solids and Structures* (2019), doi: https://doi.org/10.1016/j.ijsolstr.2019.01.018

This is a PDF file of an unedited manuscript that has been accepted for publication. As a service to our customers we are providing this early version of the manuscript. The manuscript will undergo copyediting, typesetting, and review of the resulting proof before it is published in its final form. Please note that during the production process errors may be discovered which could affect the content, and all legal disclaimers that apply to the journal pertain.

ACCEPTED MANUSCRIPT

Fully coupled thermo-viscoplastic analysis of composite structures by means of multi-scale three-dimensional finite element computations

E. Tikarrouchine[a,b], G. Chatzigeorgiou[a], Y.Chemisky[a], F. Meraghni[a,*]

[a] *Arts et Métiers ParisTech, LEM3-UMR 7239 CNRS, 4 rue Augustin Fresnel, 57078 Metz, France*

[b] *Ecole Militaire Polytechnique (EMP) BP17, Bordj El-Bahri, 16111 Alger, Algérie*

Abstract

The current paper presents a two scale Finite Element approach (FE^2), adopting the periodic homogenization method, for fully coupled thermo-mechanical processes. The aim of this work is to predict the overall response of rate-dependent, non-linear, thermo-mechanically coupled problems of 3D periodic composite structures. The material constituents implicated in the analyses obey generalized standard materials laws, while the characteristic equations of the problem (balance law, first law of thermodynamics) are expressed and satisfied in both microscopic and macroscopic scales. For the numerical implementation in both scales, the finite element commercial software ABAQUS is utilized in the framework of small strains and rotations. A set of dedicated scripts and a specially designed Meta-UMAT subroutine allow the connection between the macroscopic structure and the microscopic unit cells attached to every macroscopic integration point. The two-scale fi-

*Corresponding author

Email address: fodil.meraghni@ensam.eu (F. Meraghni)

ACCEPTED MANUSCRIPT

ACCEPTED MANUSCRIPT

nite element framework is applied to simulate thermoelastic-viscoplastic materials of complex 3D composite structures, and its capabilities are demonstrated with proper numerical examples. It is worth mentioning that the proposed computational strategy can be applied for any kind of 3D periodic microstructure and non-linear constitutive law.

Keywords: Multi-scale finite element computation, thermo-mechanical processes, periodic homogenization, thermoelastic-viscoplastic material, FE^2 method.

1. Introduction

The increasing needs of combining high strength, ductility and durability with light weight in many engineering applications, including the automotive and aerospace industry, led to the growth of the use of composite materials. The required composite materials should be able to be adopted in complicated structures with high demands in lightness, multi-functionality and durability. To design these structures it is essential to predict their thermo-mechanical response, taking into account the effect of the microstructure, as well as temperature effects arising mainly from mechanical dissipation and thermo-mechanical coupling. To satisfy such high requirements, advanced modelling and simulation approaches are required. These approaches constitute an active area of research.

The composite materials are frequently utilized in dissipative regimes (like plasticity, viscoelasticity or viscoplasticity) that could be coupled to damage phenomena Aboudi (2004); Bertram and Krawietz (2012); Anagnostou et al. (2018). Such mechanisms may be accompanied with significant temperature

ACCEPTED MANUSCRIPT

change during solicitations, that influences the material and thus the structural response. This thermo-mechanical coupling is very important to be taken into account, especially in the case of composites with thermoplastic polymer matrix, whose operational use is in temperature ranges close to the glass transition. Comprehensive thermo-mechanical couplings is naturally deduced when the constitutive equations that govern the response of the materials are derived from a consistent thermo-mechanical framework Germain (1973, 1982); Germain et al. (1983).

The scope of the present work is the prediction of the overall behavior of heterogeneous, non linear, dissipative composite structures with periodic microstructure. The developed framework should be equipped with fully coupled thermo-mechanical homogenization equations and the FE^2 computational scheme. Considering the pure mechanical response of composites, numerous multiscale models for nonlinear materials have been proposed in the literature Suquet (1987); Ponte-Castañeda (1991); Terada and Kikuchi (2001); Meraghni et al. (2002); Yu and Fish (2002); Aboudi et al. (2003); Aboudi (2004); Chaboche et al. (2005); Asada and Ohno (2007); Mercier and Molinari (2009); Khatam and Pindera (2010); Kruch and Chaboche (2011); Brenner and Suquet (2013); Mercier et al. (2012); Chatzigeorgiou et al. (2015); Charalambakis et al. (2018). In the study of periodic composite materials, the FE^2 technique appears to be an appropriate solution strategy to identify the macroscopic response of the structure, accounting for all the mechanisms observed in the heterogeneous microstructure (Feyel and Chaboche, 2000; Nezamabadi et al., 2010; Asada and Ohno, 2007; Tikarrouchine et al., 2018; Xu et al., 2018). However, very few works have been

ACCEPTED MANUSCRIPT

dedicated to thermo-mechanical coupling in the framework of FE^2 strategy. Indeed, most publications in the literature on periodic homogenization focus on purely mechanical or uncoupled thermo-mechanical problems. Özdemir et al. (2008b) proposed a multiscale uncoupled thermo-mechanical scheme as an extension of the purely thermal FE^2 solution, presented in Özdemir et al. (2008a). Chatzigeorgiou et al. (2016), have proposed a fully coupled homogenization framework, particularly suited for nonlinear dissipative composites. It has been applied to study laminate periodic composite structures using a closed form solution of the homogenization equations. Applications of fully coupled thermo-mechanical FE^2 schemes, based on the homogenization theory, have been presented for shape memory alloy (Sengupta et al., 2012) and 2D thermo-viscoplastic composites (Berthelsen et al., 2017).

The novelty and originality of the present work is the development of a fully coupled 3D thermo-mechanical homogenization framework, considering small deformations, through the FE^2 scheme, using the commercial Finite Element software ABAQUS/Standard. The proposed approach addresses the non-linear material response of composite structures in a general manner, independently of the type of constitutive laws, allowing different types of inelastic material behaviors of the composite's constituents. Illustrative numerical applications consider thermoelastic-viscoplastic material constituents. The described strategy, based on the concept of periodic homogenization, identifies the macroscopic behavior at each macroscopic integration point by attaching a periodic unit cell to it and solving the microscopic balance laws. The unit cell includes the material and geometrical characteristics of the different constituents (fiber, matrix) in the microstructure. Accordingly, a

ACCEPTED MANUSCRIPT

multilevel finite element analysis has been introduced, using an implicit resolution scheme that integrates the return mapping algorithm to solve the local constitutive equations.

The layout of the paper is as follows: in section 2, the theoretical formulation of the homogenization theory, accounting for fully-coupled thermo-mechanical processes is described, as well as the scale transition between the microscopic and the macroscopic fields. In section 3, the numerical implementation of the iterative process is detailed for a general 3D non-linear problem, including the computation of all the thermo-mechanical tangent operators. The section also discusses briefly the rate dependent constitutive law considered for the matrix phase of the numerical examples. In section 4, the multi scale FE^2 algorithm for the fully coupled thermo-mechanical problem is presented. The capabilities of the strategy are demonstrated through simulating the thermo-mechanical response of a 3D complex structure under different thermo-mechanical loading paths. The numerical analysis demonstrates that this approach is capable of rendering accurately the coupled response of non-linear, time dependent, multiscale composite structures utilizing commercial finite element analysis packages.

1.1. Notation

The following notation is adopted in this manuscript: the bar ($\overline{\bullet}$) above a symbol denotes macroscopic fields. Bold characters denote vectors or second order tensors, blackboard characters are used for fourth order tensors and regular characters represent scalar quantities. The single, twice contracted

ACCEPTED MANUSCRIPT

and dyadic products are expressed as:

$$\begin{aligned} \boldsymbol{a}\cdot\boldsymbol{b} &= a_i b_i, \qquad (\boldsymbol{A}\cdot\boldsymbol{b})_i = A_{ij}b_j, \qquad (\boldsymbol{A}\cdot\boldsymbol{B})_{ij} = A_{ik}B_{kj}, \\ \boldsymbol{A}:\boldsymbol{B} &= A_{ij}B_{ij}, \quad (\mathbb{A}:\boldsymbol{B})_{ij} = A_{ijkl}B_{kl}, \quad (\boldsymbol{A}\otimes\boldsymbol{B})_{ijkl} = A_{ij}B_{kl}. \end{aligned} \tag{1}$$

In addition, the special tensorial products are defined

$$(\mathbb{A}\,\tilde{:}\,\mathbb{B})_{ijkl} = A_{ijmn}B_{klmn}, \qquad (\boldsymbol{A}\,\tilde{\cdot}\,\boldsymbol{B})_{ij} = A_{ik}B_{jk}. \tag{2}$$

All the second order tensors considered in the manuscript are found to be symmetric ($A_{ij} = A_{ji}$) and all the fourth order tensors posses at least the minor symmetry ($A_{ijkl} = A_{jikl} = A_{ijlk}$). Consequently, all second and fourth order tensors can be respectively reduced to 6×1 and 6×6 matrices according to the Voigt notation. The operators $hyd\,(\boldsymbol{\sigma})$ and $\mathbf{dev}\,(\boldsymbol{\sigma})$ denote respectively the hydrostatic pressure and the deviatoric part of the stress tensor $\boldsymbol{\sigma}$, and $eq\,(\boldsymbol{\sigma})$ is the equivalent Von Mises stress:

$$\begin{aligned} hyd\,(\boldsymbol{\sigma}) &= \frac{1}{3}tr\,(\boldsymbol{\sigma}), \quad \mathbf{dev}\,(\boldsymbol{\sigma}) = \boldsymbol{\sigma} - hyd\,(\boldsymbol{\sigma})\,\boldsymbol{I}, \\ eq\,(\boldsymbol{\sigma}) &= \sqrt{\frac{3}{2}\,(\mathbf{dev}\,(\boldsymbol{\sigma}) : \mathbf{dev}\,(\boldsymbol{\sigma}))}. \end{aligned} \tag{3}$$

Finally, $\boldsymbol{I}$ and $\mathbb{I}$ correspond to the second and fourth order identity tensors respectively.

2. Theoretical background and scale transition principles in composites under thermo-mechanical processes

The homogenization of periodic media describes the composite as a two scale problem (micro and macro). At the macroscopic level, the deformable body occupies the volume $\overline{V}$ and is bounded by the surface $\partial\overline{V}$ with the

ACCEPTED MANUSCRIPT

outward unit vector $\overline{\boldsymbol{n}}$. Each macroscopic point is assigned with a position vector $\overline{\boldsymbol{x}}$ in $\overline{V}$ and is connected with a unit cell. At the microscopic level, the material is considered as heterogeneous and the unit cell contains information about the different constituents and their geometry. The defined periodic unit cell occupies the volume V and is bounded by the surface ∂V with the outward unit vector $\boldsymbol{n}$. Each microscopic point is assigned with a position vector $\boldsymbol{x}$ in V. The two vectors $\boldsymbol{x}$ and $\overline{\boldsymbol{x}}$ are connected through the relation $\boldsymbol{x} = \overline{\boldsymbol{x}}/\epsilon$, where ϵ is the characteristic length of the microstructure. According to the periodic homogenization theory, the separation of the overall problem in two scales provides accurate results as long as the characteristic length is close to zero, i.e. the characteristic volume of the unit cell is much smaller than the characteristic volume of the structure $\left(\mathrm{V} << \overline{V}\right)$ (Figure 1). From a practical standpoint, the minimum acceptable difference (for the validity of the proposed approach) between the size of RVE and the size of the macrosctructure depends on two factors: (i) the variation in the boundary conditions, which is related to the characteristic length of the phenomena, and (ii) the contrast in the material properties of the RVE's constituents, corresponding to the characteristic length of the microstructure. For more details see Bensoussan et al. (1978); Sanchez-Palencia (1978); Allaire (1992); Murat and Tartar (1997).

The homogenization theory seeks to identify the macroscopic response at each macroscopic point $\overline{\boldsymbol{x}}$, by computing the macroscopic thermo-mechanical fields, using information from their microscopic counterparts. This goal is achieved by introducing proper scale transition rules between the micro and the macro scale variables. According to the average theorems, when uniform

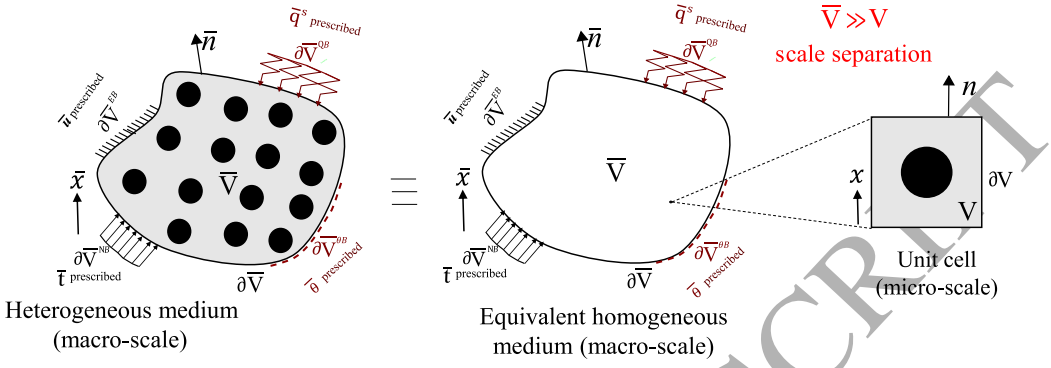

Figure 1: Schematic representation of the homogenization computational.

stress, strain, temperature gradient or heat flux is applied at the unit cell boundaries, the average (in the unit cell volume) microscopic corresponding field is equal to the applied field (Chatzigeorgiou et al., 2018). Such average fields represent the macroscopic stress, strain, temperature gradient and heat flux respectively (Hill, 1967). The relationships between the fields at the two scales are given by the following equations:

$$\overline{\boldsymbol{\sigma}} = \langle \boldsymbol{\sigma} \rangle = \frac{1}{V} \int_V \boldsymbol{\sigma} \, dV = \frac{1}{V} \int_{\partial V} \boldsymbol{\sigma} \cdot \boldsymbol{n} \otimes \boldsymbol{x} \, dS, \tag{4}$$

$$\overline{\boldsymbol{\varepsilon}} = \langle \boldsymbol{\varepsilon} \rangle = \frac{1}{V} \int_V \boldsymbol{\varepsilon} \, dV = \frac{1}{2V} \int_{\partial V} (\boldsymbol{u} \otimes \boldsymbol{n} + \boldsymbol{n} \otimes \boldsymbol{u}) \, dS, \tag{5}$$

$$\overline{\boldsymbol{\nabla}\theta} = \langle \boldsymbol{\nabla}\theta \rangle = \frac{1}{V} \int_V \boldsymbol{\nabla}\theta \, dV = \frac{1}{V} \int_{\partial V} \theta \boldsymbol{n} \, dS, \tag{6}$$

$$\overline{\boldsymbol{q}} = \langle \boldsymbol{q} \rangle = \frac{1}{V} \int_V \boldsymbol{q} \, dV = \frac{1}{V} \int_{\partial V} (\boldsymbol{q} \cdot \boldsymbol{n}) \boldsymbol{x} \, dS. \tag{7}$$

In the above expressions $\boldsymbol{\sigma}$, $\boldsymbol{\varepsilon}$, $\overline{\boldsymbol{\sigma}}$ and $\overline{\boldsymbol{\varepsilon}}$ represent the microscopic and the macroscopic stress and strain tensors respectively, while $\boldsymbol{\nabla}\theta$, $\boldsymbol{q}$, $\overline{\boldsymbol{\nabla}\theta}$ and $\overline{\boldsymbol{q}}$

ACCEPTED MANUSCRIPT

ACCEPTED MANUSCRIPT

denote the microscopic and the macroscopic temperature gradient and heat flux respectively. Moreover, $\boldsymbol{u}$ is the microscopic displacement vector. The operator $\langle \bullet \rangle$ corresponds to the mean (average) value of a microscopic field.

The motions of any macroscopic and microscopic material point $\overline{M}(\overline{\boldsymbol{x}})$ and $M(\overline{\boldsymbol{x}}, \boldsymbol{x})$ respectively are governed by the macroscopic and the microscopic equations shown in Table 1. In this Table, e and $\overline{e} = \langle e \rangle$ are the microscopic and the macroscopic internal energy per unit volume respectively, $\overline{\rho \boldsymbol{b}}$ and $\overline{\rho R}$ denote the macroscopic body forces and heat sources respectively. Moreover, η and $\overline{\eta} = \langle \eta \rangle$ denote the micro and macroscopic specific entropy. It is noted that the temperature $\overline{\theta}$ appears only with its macroscopic value, i.e. a unit cell corresponding to a macroscopic point is considered to be subjected to uniform (macroscopic) temperature. This condition arises by the zeroth order asymptotic expansion homogenization theory and its application to the thermodynamics principles (Chatzigeorgiou et al., 2016, 2018).

ACCEPTED MANUSCRIPT

ACCEPTED MANUSCRIPT

Table 1: Macroscopic and microscopic scale transition Chatzigeorgiou et al. (2016). The scalars e and $\overline{e}$ denote microscopic and macroscopic internal energy respectively, while $\overline{\rho \boldsymbol{b}}$ are the macroscopic body forces per unit volume.

Equations	Macro-scale	Micro-scale
	$\forall\, \overline{\boldsymbol{x}} \in \overline{V}$	$\forall\, \overline{\boldsymbol{x}} \in \overline{V}, \forall\, \boldsymbol{x} \in V$
Energy rate term r	$\overline{r} = \overline{\boldsymbol{\sigma}} : \dot{\overline{\boldsymbol{\varepsilon}}} - \dot{\overline{e}} = \langle r \rangle$	$r = \boldsymbol{\sigma} : \dot{\boldsymbol{\varepsilon}} - \dot{e}$
Equilibrium	$\overline{\mathbf{div}\,(\boldsymbol{\sigma})} + \overline{\rho \boldsymbol{b}} = \mathbf{0}$	$\mathbf{div}(\boldsymbol{\sigma}) = \mathbf{0}$
Energy balance	$\overline{r} - \overline{\mathbf{div}\,(\boldsymbol{q})} + \overline{\rho R} = 0$	$\mathbf{div}\,(\boldsymbol{q}) = 0$
Kinematics	$\overline{\boldsymbol{\varepsilon}} = \overline{\mathbf{grad}_{sym}\,(\boldsymbol{u})}$	$\boldsymbol{\varepsilon} = \mathbf{grad}_{sym}\,(\boldsymbol{u})$
Constitutive law	$\overline{\boldsymbol{\sigma}} \equiv \overline{\boldsymbol{\sigma}}\left(\overline{\boldsymbol{x}}, \overline{\boldsymbol{\varepsilon}}, \overline{\theta}\right)$	$\boldsymbol{\sigma} \equiv \boldsymbol{\sigma}\left(\overline{\boldsymbol{x}}, \overline{\theta}, \boldsymbol{x}, \boldsymbol{\varepsilon}\right)$
Strain energy rate	$\dot{\overline{W}}_{\varepsilon} = \overline{\boldsymbol{\sigma}} : \dot{\overline{\boldsymbol{\varepsilon}}}$	$\dot{W}_{\varepsilon} = \boldsymbol{\sigma} : \dot{\boldsymbol{\varepsilon}}$
Entropy inequality	$\overline{\theta}\dot{\overline{\eta}} + \overline{r} - \frac{\overline{\boldsymbol{q}}}{\overline{\theta}} \cdot \overline{\boldsymbol{\nabla}\theta} \geq 0$	$\overline{\theta}\dot{\eta} + r - \frac{\boldsymbol{q}}{\overline{\theta}} \cdot \boldsymbol{\nabla}\theta \geq 0$

The following subsections of this section describe in a more precise manner the fully-coupled thermo-mechanical problem in the two scales, the macroscopic and the microscopic.

2.1. Macroscopic problem

The deformable body $\overline{V}$ presented in Figure 1 is subjected to thermo-mechanical conditions at the boundary surface of the body $\partial\overline{V}$. Neglecting inertia effects, the conservation of linear momentum and the energy balance

ACCEPTED MANUSCRIPT

equation are written at the macroscopic scale as

$$\overline{\mathbf{div}}\,(\overline{\boldsymbol{\sigma}}) + \overline{\rho \boldsymbol{b}} = \mathbf{0}, \tag{8}$$

$$\overline{r} - \overline{\mathbf{div}}\,(\overline{\boldsymbol{q}}) + \overline{\rho R} = 0. \tag{9}$$

Moreover, the kinematics and temperature gradient relations state that

$$\overline{\boldsymbol{\varepsilon}} = \overline{\mathbf{grad}}_{sym}(\overline{\boldsymbol{u}}) \qquad \text{in } \overline{V}. \tag{10}$$

$$\overline{\boldsymbol{\nabla}\theta} = \overline{\mathbf{grad}}(\overline{\theta}) \qquad \text{in } \overline{V}. \tag{11}$$

The conservation laws are generally accompanied by Dirichlet type, Neumann type or mixed thermo-mechanical boundary conditions: Generally speaking, prescribed displacement $\overline{\boldsymbol{u}}^{prescribed}$ can be applied on the surface $\overline{\partial V}^{EB}$, external traction $\overline{\boldsymbol{t}}$ can be imposed on the surface $\overline{\partial V}^{NB}$, prescribed temperature $\overline{\theta}^{prescribed}$ can be considered on the surface $\overline{\partial V}^{\theta B}$ and external heat flux scalar $\overline{q}^{s}$ can be applied on the surface $\overline{\partial V}^{QB}$,

$$\begin{cases} \overline{\boldsymbol{u}} = \overline{\boldsymbol{u}}^{prescribed} & \text{on } \overline{\partial V}^{EB}, \\ \overline{\boldsymbol{\sigma}} \cdot \overline{\boldsymbol{n}} = \overline{\boldsymbol{t}} & \text{on } \overline{\partial V}^{NB}, \\ \overline{\theta} = \overline{\theta}^{prescribed} & \text{on } \overline{\partial V}^{\theta B}, \\ -\overline{\boldsymbol{q}} \cdot \overline{\boldsymbol{n}} = \overline{q}^{s} & \text{on } \overline{\partial V}^{QB}. \end{cases} \tag{12}$$

The previously defined surfaces are parts of the overall boundary surface $\overline{\partial V}$, satisfying the conditions

$$\overline{\partial V}^{EB} \cup \overline{\partial V}^{NB} = \overline{\partial V}, \tag{13}$$

$$\overline{\partial V}^{\theta B} \cup \overline{\partial V}^{QB} = \overline{\partial V}. \tag{14}$$

ACCEPTED MANUSCRIPT

If convection is considered (Robin type boundary conditions), then a mixed-type of thermal boundary condition, of the form

$$\overline{q}^c = h_c \left(\overline{\theta}_0 - \overline{\theta}\right), \tag{15}$$

can be assigned to a part of the boundary surface. In the last relation, $\overline{q}^c = \dfrac{\dot{\overline{Q}}}{\overline{A}}$ is the prescribed heat flux, with $\dot{\overline{Q}}$ denoting the heat transferred per unit time and $\overline{A}$ denoting the heat transfer area of the surface. h_c is the convective heat transfer coefficient of the process, which is a quantitative characteristic of the heat transfer between a fluid medium and the surface flowed over by the fluid. Moreover, $\overline{\theta}_0$ and $\overline{\theta}$ are the temperatures of the surrounding fluid and the solid surface respectively.

2.2. Microscopic problem

As already mentioned previously, a periodic unit cell is assigned at every macroscopic point, accounting for the geometrical and material characteristics of the microstructure. As defined by the zeroth order asymptotic expansion theory, at such unit cells the microscopic equilibrium equation is solved considering constant macroscopic temperature at every point of the unit cell. The energy rate term r and the thermomechanical tangent moduli are also identified for the same macroscopic temperature. Considering the pure thermal problem, the microscopic energy balance is reduced to steady state heat conduction equation. In that sense, the coupled thermomechanical and the pure thermal problems can be treated separately (Chatzigeorgiou et al., 2016). Mathematically speaking, the underlying hypothesis behind this condition is that the temperature converges strongly to a specific value, enforcing a uniform value (equal to the macroscopic temperature) at the unit

ACCEPTED MANUSCRIPT

cell corresponding to a macroscopic point. On the other hand, the gradient of the temperature converges weakly, which implies that the microscopic temperature gradient varies inside the periodic unit cell and its average value can be defined as the macroscopic temperature gradient at the macroscopic point Chatzigeorgiou et al. (2018).

A way to relax this uncoupling for the microscopic problem is to employ higher order homogenization theories. In that way, one can also account for the size effects. While mathematically such approach is valid (see for instance Dong et al., 2017 for thermoelastic materials), the thermodynamic implications are not fully clear. The second order homogenization in composites with purely mechanical response introduces macroscopic strain gradients that enter directly into the overall constitutive behavior Kouznetsova et al. (2002). This behavior is compatible with existent thermodynamic frameworks Forest (2009). On the other hand, the second order theory for thermo-mechanically coupled processes introduces additional dependence of the stress on the temperature gradient Dong et al. (2017). From a physical point of view such relation is problematic and is not allowed in existent thermodynamic theories accounting for internal variables Coleman and Gurtin (1967); Germain et al. (1983).

In this work the zeroth order homogenization theory, as described in Chatzigeorgiou et al. (2016), is utilized. The assumption $\theta = \overline{\theta}$, adopted in that work, predicts thermal strains which are in full agreement with established techniques in the micromechanics community (for instance, the well known and widely utilized Levin's formula for computing the thermal expansion coefficients tensor of a composite), as well as with other periodic

ACCEPTED MANUSCRIPT

homogenization studies in the cases of thermoelasticity Ene (1983); Temizer (2012) and thermoviscoelasticity Yu and Fish (2002).

It is worth mentioning that the proposed micro-macro temperature relation allows to establish a macroscopic representation of the second law of thermodynamics, as illustrated in Chatzigeorgiou et al. (2016). A more relaxed micro-macro temperature relation, as the one proposed by Sengupta et al. (2012), does not provide a clear definition for the macro-entropy and a macroscopic representation of the dissipation due to heat conduction. It should be also noted that the homogenization framework obtained by the zeroth order asymptotic expansion method does not account for size effects, i.e. the size of the RVE does not influence the macroscopic response. Size effects may appear either due to not sufficiently small microstructure or due to instability related phenomena, like strain localization, interphase debonding etc. Under these conditions strain gradient effects may be quite important and should be taken into account through higher order homogenization theories.

Microscopic coupled thermo-mechanical problem

At each macroscopic point, the corresponding unit cell serves at identifying the microscopic variables whose average values provide the macroscopic fields. In the mechanical part of the problem, the microscopic stress is evaluated through the microscopic equilibrium equation, in which the macroscopic strain and temperature are used as input data. Once the microscopic mechanical problem is solved, the macroscopic stress is evaluated by averaging the microscopic stresses over the unit cell. As additional information one obtains also the macroscopic energy rate term $\overline{r}$, which is equal to the average value of its microscopic counterparts. The energy rate term r depends

ACCEPTED MANUSCRIPT

exclusively on variables linked with the stress, the strain and the absolute temperature, thus it can be computed once the microscopic equilibrium is solved. Information about the microscopic temperature gradients are obtained from the microscopic pure thermal problem and they are not required at this stage.

The microscopic equilibrium system is solved under uniform macroscopic temperature $\overline{\theta}$ and periodic displacement boundary conditions. The periodicity condition implies that the displacement field $\boldsymbol{u}$ of any microscopic material point located in the position vector $\boldsymbol{x}$ is described by an affine part, plus a periodic fluctuation $\widetilde{\boldsymbol{u}}$,

$$\boldsymbol{u}\left(\overline{\boldsymbol{x}},\boldsymbol{x},t\right)=\overline{\boldsymbol{\varepsilon}}\left(\overline{\boldsymbol{x}},t\right)\cdot\boldsymbol{x}+\widetilde{\boldsymbol{u}}\left(\overline{\boldsymbol{x}},\boldsymbol{x},t\right). \tag{16}$$

The periodic fluctuating part $\widetilde{\boldsymbol{u}}$ takes the same value on each pair of opposite parallel sides of the unit cell. The strain average produced by $\widetilde{\boldsymbol{u}}$ is null. However, the total microscopic strain average is equal to the macroscopic strain:

$$\boldsymbol{\varepsilon}\left(\boldsymbol{u}\right)=\overline{\boldsymbol{\varepsilon}}+\boldsymbol{\varepsilon}\left(\widetilde{\boldsymbol{u}}\right), \tag{17}$$

$$\left\langle\boldsymbol{\varepsilon}\left(\widetilde{\boldsymbol{u}}\right)\right\rangle=\frac{1}{V}\int_{V}\boldsymbol{\varepsilon}\left(\widetilde{\boldsymbol{u}}\right)\,dV=\boldsymbol{0}, \tag{18}$$

$$\left\langle\boldsymbol{\varepsilon}\left(\boldsymbol{u}\right)\right\rangle\;=\overline{\boldsymbol{\varepsilon}}\;+\left\langle\boldsymbol{\varepsilon}\left(\widetilde{\boldsymbol{u}}\right)\right\rangle\;=\overline{\boldsymbol{\varepsilon}}. \tag{19}$$

In addition, the traction vector $\boldsymbol{\sigma}.\boldsymbol{n}$ is anti periodic. The microscopic equilibrium is free of body forces and the complete mechanical system of equations

ACCEPTED MANUSCRIPT

is formulated as follows:

$$\begin{cases} \mathbf{div}\left(\boldsymbol{\sigma}\left(\overline{\boldsymbol{x}},\overline{\theta},\boldsymbol{x},\boldsymbol{\varepsilon}\right)\right)=\mathbf{0} & \forall \boldsymbol{x}\in V, \\ \boldsymbol{\sigma}=\boldsymbol{F}\left(\overline{\boldsymbol{x}},\overline{\theta},\boldsymbol{x},\boldsymbol{\varepsilon}\right) & \forall \boldsymbol{x}\in V, \\ \theta=\overline{\theta} & \forall \boldsymbol{x}\in V, \\ \boldsymbol{u}_i\,-\,\boldsymbol{u}_j=\overline{\boldsymbol{\varepsilon}}\cdot\left(\boldsymbol{x}_i\,-\,\boldsymbol{x}_j\right) & \forall \boldsymbol{x}\in \partial V. \end{cases} \tag{20}$$

In the boundary condition $(20)_4$, $\boldsymbol{u}_i$ and $\boldsymbol{u}_j$ are the displacement vectors at the positions $\boldsymbol{x}_i$ and $\boldsymbol{x}_j$ respectively, which define a pair of parallel opposite material points on the unit cell boundary. The solution of the above system of equations using incremental approach is detailed in section 3.

Pure thermal problem: macroscopic thermal conductivity

The zeroth order homogenization theory reduces the microscopic energy balance to the steady state heat conduction equation

$$\mathbf{div}\left(\boldsymbol{q}\left(\overline{\boldsymbol{x}},\overline{\theta},\boldsymbol{x}\right)\right)=0, \quad \text{with} \quad \boldsymbol{q}=-\boldsymbol{\kappa}\cdot\boldsymbol{\nabla}\theta, \qquad \forall \boldsymbol{x}\in V. \tag{21}$$

Frequently in solids the thermal conductivity tensor $\boldsymbol{\kappa}$ is considered constant, independent of the temperature. The energy balance equation (21) is solved under periodic temperature conditions. The periodicity assumption implies that the temperature field θ is equal to the sum of a macroscopic part $\overline{\boldsymbol{\nabla}\theta}$ and a periodic fluctuation part $\widetilde{\theta}$.

$$\theta\left(\overline{\boldsymbol{x}},\boldsymbol{x},t\right)=\overline{\boldsymbol{\nabla}\theta}\left(\overline{\boldsymbol{x}},t\right)\cdot\boldsymbol{x}+\widetilde{\theta}\left(\overline{\boldsymbol{x}},\boldsymbol{x},t\right). \tag{22}$$

The periodic fluctuation part takes the same value at each parallel opposite point on the unit cell boundary. By applying the gradient operator, equation (22) gives

$$\boldsymbol{\nabla}\theta=\overline{\boldsymbol{\nabla}\theta}+\widetilde{\boldsymbol{\nabla}\theta}. \tag{23}$$

ACCEPTED MANUSCRIPT

Averaging (23) yields equation (6). As an additional constraint, the heat flux vector $-\boldsymbol{q}\cdot\boldsymbol{n}$ should be anti periodic.

The microscopic energy balance in the form of (21) is a linear problem that can be solved once in order to provide the macroscopic thermal conductivity tensor $\overline{\boldsymbol{\kappa}}$. Indeed, substituting equation (23) in (21) gives

$$\mathbf{div}\left(\boldsymbol{\kappa}\cdot\left(\overline{\boldsymbol{\nabla}\theta}+\widetilde{\boldsymbol{\nabla}\theta}\right)\right)=0. \tag{24}$$

Assuming that the macroscopic temperature gradient $\overline{\boldsymbol{\nabla}\theta}$ is known, the solution of the above homogeneous equation is written under the following form

$$\widetilde{\theta}=\boldsymbol{\psi}^{\theta}\cdot\overline{\boldsymbol{\nabla}\theta}, \tag{25}$$

where the vector $\boldsymbol{\psi}^{\theta}$ is periodic and is called the corrector vector. Substituting (25) in (24) yields

$$\overline{\boldsymbol{\nabla}\theta}\,\mathbf{div}\left(\left[\boldsymbol{\kappa}+\boldsymbol{\kappa}\,\tilde{\cdot}\,\boldsymbol{\nabla}\boldsymbol{\psi}^{\theta}\right]^{T}\right)=0. \tag{26}$$

The last expression must be satisfied for any arbitrary value of the macroscopic variable $\overline{\boldsymbol{\nabla}\theta}$. This implies that the corrector vector has to satisfy the linear equation

$$\mathbf{div}\left(\left[\boldsymbol{\kappa}+\boldsymbol{\kappa}\,\tilde{\cdot}\,\boldsymbol{\nabla}\boldsymbol{\psi}^{\theta}\right]^{T}\right)=0. \tag{27}$$

With the help of equations (23) and (25), the heat flux $(21)_2$ is written as

$$\boldsymbol{q}=-\boldsymbol{\kappa}\cdot\boldsymbol{A}^{\kappa}\cdot\overline{\boldsymbol{\nabla}\theta}, \tag{28}$$

where

$$\boldsymbol{A}^{\kappa}=\boldsymbol{I}+\left[\boldsymbol{\nabla}\boldsymbol{\psi}^{\theta}\right]^{T}. \tag{29}$$

ACCEPTED MANUSCRIPT

Averaging the last expression over the unit cell and assuming that the macroscopic heat flux is expressed by a similar constitutive law with its microscopic counterpart,

$$\overline{\boldsymbol{q}} = -\overline{\boldsymbol{\kappa}} \cdot \overline{\boldsymbol{\nabla}\theta}, \tag{30}$$

yields the macroscopic thermal conductivity tensor $\overline{\boldsymbol{\kappa}}$,

$$\overline{\boldsymbol{\kappa}} = \langle \boldsymbol{\kappa} \cdot \boldsymbol{A}^k \rangle. \tag{31}$$

While the present article examines composites with constant thermal conductivities at the constituents of the microstructure, the proposed framework allows to adopt temperature varied thermal conductivities. In such case, the condition $\theta = \overline{\theta}$ of the zeroth order asymptotic expansion homogenization theory enforces to consider that the microscopic thermal conductivities should be expressed as functions of the macroscopic temperature.

The microscopic pure thermal problem is linear and no iterative procedure is required for its solution. The numerical computation of the macroscopic thermal conductivity is discussed in section 4.

3. Numerical implementation: iterative process and tangent operators

The resolution of the fully coupled thermo-mechanical homogenization framework for composites consisting of generalized standard dissipative materials requires robust numerical procedure. Before proceeding to the numerical schemes, the following definitions of increments and iterations are introduced:

ACCEPTED MANUSCRIPT

In incremental schemes for nonlinear materials, the variable of time is discretized in various steps. Usually the time discretization follows a backward Euler numerical procedure. During a time step, a nonlinear system of equations is solved iteratively. Within time step, iterations are usually necessary to find the correct values that satisfies the system of equations. Thus, two notations need to be defined:

- The symbol Δ before a variable denotes the time increment of the variable between two consecutive time steps. The updated value of the variable ϕ is expressed from the previous time step n by the relation

$$\phi^{n+1} = \phi^n + \Delta\phi.$$

- The symbol δ before a variable denotes the iteration increment of the variable at a specific time increment. The current values of the variable ϕ and its time increment $\Delta\phi$ are updated from iteration k to iteration $k+1$ per

$$\phi^{(n+1)(k+1)} = \phi^{(n+1)(k)} + \delta\phi,$$
$$\Delta\phi^{(n+1)(k+1)} = \Delta\phi^{(n+1)(k)} + \delta\phi.$$

An additional complexity of the homogenization procedure compared to standard homogeneous materials is that the solution of the unit cell problem strongly depends on the numerical solution of the macroscopic analysis and vise versa in a coupled way. In other words, the problems in the two scales (macroscopic and microscopic) should be solved simultaneously, through iterative schemes. Indeed:

- The unit cell problem at every macroscopic point is utilized for the evaluation of the macroscopic stress $\overline{\boldsymbol{\sigma}}$, the macroscopic energy rate

ACCEPTED MANUSCRIPT

term $\overline{r}$ and the macroscopic thermomechanical tangent moduli (defined later in this section). These quantities are computed through finite element calculations considering periodicity displacement conditions at the unit cell.

- The macroscopic analysis feeds back the microscopic problems with the updated time increments of the macroscopic strain $\Delta\overline{\boldsymbol{\varepsilon}}$ and the temperature $\Delta\overline{\theta}$, as well as the history of all macroscopic fields.

The numerical solution steps and the iterative procedures are described in the next subsections for both scales.

3.1. Macroscopic problem

The balance laws, kinematics and boundary conditions at the macroscopic scale, expressed by (8)-(11), (12) and/or (15), should be accompanied with a macroscopic constitutive laws to be able to find the solution. For the case of nonlinear materials and especially in nonlinear homogenization procedures, analytical expressions for the constitutive response are very seldom and usually only incremental formalisms can be provided. At a specific time increment, the macroscopic stress ($\overline{\boldsymbol{\sigma}}$) and energy rate term ($\overline{r}$) iteration increments are linked with the iteration increments of the macroscopic strain ($\overline{\boldsymbol{\varepsilon}}$) and temperature ($\overline{\theta}$) through the relations

$$\delta\overline{\boldsymbol{\sigma}} = \overline{\mathbb{D}}^{\varepsilon} : \delta\overline{\boldsymbol{\varepsilon}} + \overline{\boldsymbol{D}}^{\theta}\delta\overline{\theta}, \qquad \delta\overline{r} = \overline{\boldsymbol{R}}^{\varepsilon} : \delta\overline{\boldsymbol{\varepsilon}} + \overline{R}^{\theta}\delta\overline{\theta}, \tag{32}$$

where

$$\delta\overline{\boldsymbol{\varepsilon}} = \overline{\mathbf{grad}}_{sym}\delta\overline{\boldsymbol{u}}. \tag{33}$$

ACCEPTED MANUSCRIPT

In the above expressions $\overline{\mathbb{D}}^{\varepsilon}$, $\overline{\boldsymbol{D}}^{\theta}$, $\overline{\boldsymbol{R}}^{\varepsilon}$ and $\overline{R}^{\theta}$ are the thermo-mechanical macroscopic tangent operators. These operators are computed at every macroscopic point and at every macroscopic iteration increment from the resolution of a unit cell problem. This problem is described in the next subsection. The final constitutive relation, connecting the iteration increments of the macroscopic heat flux and the macroscopic temperature gradient is

$$\delta\overline{\boldsymbol{q}} = -\overline{\boldsymbol{\kappa}} \cdot \overline{\boldsymbol{\nabla}\delta\theta}, \qquad \text{where } \overline{\boldsymbol{\nabla}\delta\theta} = \overline{\mathbf{grad}\,\delta\theta}. \tag{34}$$

It is recalled that the macroscopic thermal conductivity tensor is considered constant and is computed once from equation (31). With the help of these increments, the stress, the energy term and the heat flux are iteratively updated through the linearized expressions

$$\begin{aligned} \overline{\boldsymbol{\sigma}}^{(n+1)(k+1)} &= \overline{\boldsymbol{\sigma}}^{(n+1)(k)} + \delta\overline{\boldsymbol{\sigma}}, \quad \overline{r}^{(n+1)(k+1)} = \overline{r}^{(n+1)(k)} + \delta\overline{r}, \\ \overline{\boldsymbol{q}}^{(n+1)(k+1)} &= \overline{\boldsymbol{q}}^{(n+1)(k)} + \delta\overline{\boldsymbol{q}} = -\overline{\boldsymbol{\kappa}} \cdot (\overline{\boldsymbol{\nabla}\theta}^{(n+1)(k)} + \overline{\boldsymbol{\nabla}\delta\theta}). \end{aligned} \tag{35}$$

The values of $\overline{\boldsymbol{\sigma}}$ and $\overline{r}$ at every macroscopic point and iteration increment are provided by the solution of the microscopic unit cell problem, which is explained in details in the next subsection.

With the updated values, the equilibrium (8) and energy balance (9) equations are written as

$$\begin{aligned} \overline{\mathbf{div}\boldsymbol{\sigma}}^{(n+1)(k+1)} + \overline{\rho\boldsymbol{b}} &= \mathbf{0}, \\ \overline{r}^{(n+1)(k+1)} - \overline{\mathbf{div}\boldsymbol{q}}^{(n+1)(k+1)} + \overline{\rho R} &= 0. \end{aligned} \tag{36}$$

The latter linearized system of equations accepts only the iteration increments of the displacements $\delta\overline{\boldsymbol{u}}$ and the temperatures $\delta\overline{\theta}$ as unknowns. Its

ACCEPTED MANUSCRIPT

resolution provides eventually the time increments of the macroscopic strains $\Delta\overline{\boldsymbol{\varepsilon}}$ and the temperature $\Delta\overline{\theta}$ at the complete macrostructure. These time increments and the previous state of all macroscopic fields are the basic input to the unit cells attached to every macroscopic point.

Equations (36) are solved iteratively until $\delta\overline{\boldsymbol{u}}$ and $\delta\overline{\theta}$ at every macroscopic point converge with a predefined tolerance.

3.2. Unit cell problem

Having obtained the history of the macroscopic fields, as well as the time increments of the macroscopic strains and temperature at a macroscopic point, its attached unit cell is solved separately in two parts: The first part is devoted to the computation of the macroscopic stress $\overline{\boldsymbol{\sigma}}$ and the energy rate term $\overline{r}$ and the second part is dedicated to the calculation of the macroscopic tangent operators.

First part of unit cell problem: macroscopic stress

In the first part, the microscopic mechanical system of equations (20) is solved for the time step t_{n+1} under uniform temperature $\overline{\theta}^{(n+1)} = \overline{\theta}^{n} + \Delta\overline{\theta}$, by using as additional input the macroscopic strain $\overline{\boldsymbol{\varepsilon}}^{n+1} = \overline{\boldsymbol{\varepsilon}}^{n} + \Delta\overline{\boldsymbol{\varepsilon}}$ and the values of all fields (macroscopic and microscopic) at the previous time step t_n. It is noted that the exponents $n+1$ and n denote quantities defined at time steps t_{n+1} and t_n respectively. In a return mapping algorithmic scheme, the strain and temperature do not evolve with iterations, since these are provided as input from the finite element solution of the balance equations (here they are computed from the macroscopic analysis). In that sense, $\delta\overline{\boldsymbol{\varepsilon}} = \mathbf{0}$ and $\delta\overline{\theta} = 0$.

ACCEPTED MANUSCRIPT

The microscopic stress tensor at the time step $n+1$ can be expressed in linearized form as follows:

$$\boldsymbol{\sigma}^{(n+1)(k+1)} = \boldsymbol{\sigma}\left(\overline{\boldsymbol{x}}, \overline{\theta}^{n+1}, \boldsymbol{x}, \boldsymbol{\varepsilon}^{(n+1)(k)}\right) + \mathbb{D}^{\varepsilon} : \mathbf{grad}_{sym}\delta\boldsymbol{u}, \tag{37}$$

where $\boldsymbol{\varepsilon}$ is the microscopic strain computed in the previous microscopic iteration step and $\mathbb{D}^{\varepsilon}$ denotes the fourth order mechanical tangent operator tensor. The microscopic stress $\boldsymbol{\sigma}$ and the microscopic thermomechanical tangent moduli are obtained through the constitutive law of the material under consideration. In finite element programs like ABAQUS the constitutive law is numerically defined with the help of a user material (UMAT) subroutine. Algorithmic structures of such subroutines for various types of constitutive laws are presented in Chatzigeorgiou et al. (2018).

Combining all the above expressions, the mechanical system (20) is written in the linearized form as

$$\begin{cases} \mathbf{div}\boldsymbol{\sigma}^{(n+1)(k+1)} = \mathbf{0} & \forall \boldsymbol{x} \in V, \\ \boldsymbol{u}_i - \boldsymbol{u}_j = \overline{\boldsymbol{\varepsilon}}^{n+1} \cdot (\boldsymbol{x}_i - \boldsymbol{x}_j) & \forall \boldsymbol{x} \in \partial V. \end{cases} \tag{38}$$

The latter is a linearized system with unknown displacement increment $\delta\boldsymbol{u}$ and it has a unique solution as long as $\mathbb{D}^{\varepsilon}$ is positive definite. Equation (38) is solved iteratively, until $\delta\boldsymbol{u}$ at every microscopic point converges to a predefined tolerance. Once the convergence is achieved, the computation of the microscopic displacements $\boldsymbol{u}$, strains $\boldsymbol{\varepsilon}$ and stresses $\boldsymbol{\sigma}$ follows. Additionally, one can also compute the microscopic energy rate term r at every unit cell point, without passing to the energy balance equation. Consequently, the macroscopic stress $\overline{\boldsymbol{\sigma}}$ and the macroscopic energy rate term $\overline{r}$ are computed by averaging their microscopic counterparts.

ACCEPTED MANUSCRIPT

It is noted that the computation of the microscopic heat flux $\boldsymbol{q}$ is not required for the macroscopic analysis, since the macroscopic thermal conductivity $\overline{\boldsymbol{\kappa}}$ is constant for specific unit cell geometric and material characteristics.

Second part of unit cell problem: tangent operators

The second part is dedicated to the calculation of the macroscopic tangent operators. For this part of the analysis, the macroscopic strain and temperature iteration increments are assumed non-zero. In that case, the iteration increments of the microscopic stress and of the energy rate term r are expressed as

$$\delta\boldsymbol{\sigma} = \mathbb{D}^{\varepsilon} : \delta\boldsymbol{\varepsilon} + \boldsymbol{D}^{\theta}\,\delta\overline{\theta}, \qquad \delta r = \boldsymbol{R}^{\varepsilon} : \delta\boldsymbol{\varepsilon} + R^{\theta}\delta\overline{\theta}, \tag{39}$$

where

$$\delta\boldsymbol{\varepsilon} = \delta\overline{\boldsymbol{\varepsilon}} + \mathbf{grad}_{sym}\delta\tilde{\boldsymbol{u}}. \tag{40}$$

The microscopic thermo-mechanical tangent operators $\mathbb{D}^{\varepsilon}$, $\boldsymbol{D}^{\theta}$, $\boldsymbol{R}^{\varepsilon}$ and R^{θ} are instantaneous tangent tensors that are calculated at the end of the iterative procedure of the first part of the unit cell problem. Thus, in the second part they are considered constant and the microscopic equilibrium

$$\mathbf{div}\,(\delta\boldsymbol{\sigma}) = \mathbf{0}, \tag{41}$$

or (after combining equations (41) and (39))

$$\mathbf{div}\left(\mathbb{D}^{\varepsilon} : \delta\overline{\boldsymbol{\varepsilon}} + \boldsymbol{D}^{\theta}\,\delta\overline{\theta} + \mathbb{D}^{\varepsilon} : \mathbf{grad}_{sym}\delta\tilde{\boldsymbol{u}}\right) = \mathbf{0}, \tag{42}$$

is a linear problem with periodic boundary conditions in terms of $\delta\tilde{\boldsymbol{u}}$. Its solution can be written in the form (Ene, 1983)

$$\delta\tilde{\boldsymbol{u}} = \delta\overline{\boldsymbol{\varepsilon}} : \boldsymbol{\chi}^{\varepsilon} + \delta\overline{\theta}\;\boldsymbol{\chi}^{\theta}. \tag{43}$$

ACCEPTED MANUSCRIPT

In the latter expression, the third order tensor $\boldsymbol{\chi}^{\varepsilon}$ and the vector $\boldsymbol{\chi}^{\theta}$ are periodic and are called corrector terms. Substituting equation (43) in (42) yields

$$\delta\overline{\boldsymbol{\varepsilon}} : \mathbf{div}\left([\mathbb{D}^{\varepsilon} + \mathbb{D}^{\varepsilon} \,\tilde{:}\, \mathbf{grad}\boldsymbol{\chi}^{\varepsilon}]^{T}\right) + \delta\overline{\theta}\ \mathbf{div}\left(\boldsymbol{D}^{\theta} + \mathbb{D}^{\varepsilon} : \mathbf{grad}\boldsymbol{\chi}^{\theta}\right) = \mathbf{0}. \quad (44)$$

The above homogeneous equation has a solution for arbitrary values of the macroscopic variables $\delta\overline{\boldsymbol{\varepsilon}}$ and $\delta\overline{\theta}$ only if the corrector terms satisfy the linear equations

$$\mathbf{div}\left([\mathbb{D}^{\varepsilon} + \mathbb{D}^{\varepsilon} \,\tilde{:}\, \mathbf{grad}\boldsymbol{\chi}^{\varepsilon}]^{T}\right) = \mathbf{0}, \qquad \mathbf{div}\left(\boldsymbol{D}^{\theta} + \mathbb{D}^{\varepsilon} : \mathbf{grad}\boldsymbol{\chi}^{\theta}\right) = \mathbf{0}. \quad (45)$$

From this linear uncoupled system one obtains $\mathbf{grad}_{sym}\boldsymbol{\chi}^{\varepsilon}$ and $\mathbf{grad}\boldsymbol{\chi}^{\theta}$. Using equations (43), the increments of the microscopic fields are written in the following form

$$\begin{aligned}
\delta\boldsymbol{\varepsilon} &= \mathbb{A}^{\varepsilon} : \delta\overline{\boldsymbol{\varepsilon}} + \boldsymbol{A}^{\theta}\delta\overline{\theta}, \\
\delta\boldsymbol{\sigma} &= \mathbb{D}^{\varepsilon} : \mathbb{A}^{\varepsilon} : \delta\overline{\boldsymbol{\varepsilon}} + [\boldsymbol{D}^{\theta} + \mathbb{D}^{\varepsilon} : \boldsymbol{A}^{\theta}]\delta\overline{\theta}, \\
\delta r &= \boldsymbol{R}^{\varepsilon} : \mathbb{A}^{\varepsilon} : \delta\overline{\boldsymbol{\varepsilon}} + [R^{\theta} + \boldsymbol{R}^{\varepsilon} : \boldsymbol{A}^{\theta}]\delta\overline{\theta},
\end{aligned} \quad (46)$$

where

$$\mathbb{A}^{\varepsilon} = \mathbb{I} + \mathbb{I} \,\tilde{:}\, \mathbf{grad}\boldsymbol{\chi}^{\varepsilon}, \qquad \boldsymbol{A}^{\theta} = \mathbf{grad}_{sym}\boldsymbol{\chi}^{\theta}. \quad (47)$$

Averaging $(46)_{1,2}$ over the unit cell volume yields that the macroscopic thermo-mechanical tangent operators are given by the expressions

$$\begin{aligned}
\overline{\mathbb{D}}^{\varepsilon} &= \langle \mathbb{D}^{\varepsilon} : \mathbb{A}^{\varepsilon} \rangle, \quad \overline{\boldsymbol{D}}^{\theta} = \langle \boldsymbol{D}^{\theta} + \mathbb{D}^{\varepsilon} : \boldsymbol{A}^{\theta} \rangle, \\
\overline{\boldsymbol{R}}^{\varepsilon} &= \langle \boldsymbol{R}^{\varepsilon} : \mathbb{A}^{\varepsilon} \rangle, \quad \overline{R}^{\theta} = \langle R^{\theta} + \boldsymbol{R}^{\varepsilon} : \boldsymbol{A}^{\theta} \rangle.
\end{aligned} \quad (48)$$

The above described incremental iterative procedure for the two parts of the microscopic unit cell problem requires a well designed constitutive law

ACCEPTED MANUSCRIPT

for each material phase of the microstructure. In general, this constitutive law, implemented in the form of a return mapping algorithm scheme, should provide i) the stress $\boldsymbol{\sigma}$ and the internal state variables for given strain $\boldsymbol{\varepsilon}$ and temperature θ and ii) the thermo-mechanical tangent operators $\mathbb{D}^{\varepsilon}$, $\boldsymbol{D}^{\theta}$, $\boldsymbol{R}^{\varepsilon}$ and R^{θ}.

Without loss of generality, the studied examples in this manuscript consider two types of constitutive response: thermoelastic for the fibers and thermoelastic-viscoplastic with isotropic hardening for the matrix phase. While the numerical implementation details are not shown here, still for the reader's convenience the essential points of the matrix material behavior are briefly discussed in the following subsection.

3.3. Thermoelastic-viscoplastic behavior with isotropic hardening

The thermoelastic-viscoplastic constitutive law chosen for the matrix phase of the studied examples is formulated in the context of small deformations and small rotations theory. In this framework the total strain $\boldsymbol{\varepsilon}$ is additively decomposed into an elastic part $\boldsymbol{\varepsilon}_e$, a viscoplastic part $\boldsymbol{\varepsilon}_p$ and a thermal part $\boldsymbol{\varepsilon}_{th}$:

$$\boldsymbol{\varepsilon} = \boldsymbol{\varepsilon}_e + \boldsymbol{\varepsilon}_p + \boldsymbol{\varepsilon}_{th}, \qquad \boldsymbol{\varepsilon}_{th} = \boldsymbol{\alpha}\left(\theta - \theta^i\right), \tag{49}$$

where $\boldsymbol{\alpha}$ is the second order thermal expansion coefficient tensor and θ^i is the initial temperature. From a thermodynamical point of view, the state laws for a generalized standard material are obtained by differentiating the Helmholtz free energy potential with respect to the state variables. The chosen state variables for the constitutive law in discussion are the total strain $\boldsymbol{\varepsilon}$, the temperature θ, and the internal state variables $\boldsymbol{V}_k$ that consist of the viscoplastic strain $\boldsymbol{\varepsilon}_p$ and the effective viscoplastic strain p. The Helmholtz free

ACCEPTED MANUSCRIPT

energy potential corresponding to a thermoelastic-viscoplastic material with isotropic hardening takes the form Lemaitre and Chaboche (1990); Praud et al. (2017); Chatzigeorgiou et al. (2018)

$$\begin{aligned}\psi = \psi\left(\boldsymbol{\varepsilon}, \theta, \boldsymbol{V}_k\right) = \psi\left(\boldsymbol{\varepsilon}, \theta, \boldsymbol{\varepsilon}_p, p\right) \\ = \underbrace{\frac{1}{2}\left[\boldsymbol{\varepsilon} - \boldsymbol{\varepsilon}_p - \boldsymbol{\alpha}(\theta - \theta^i)\right] : \mathbb{C}_e : \left[\boldsymbol{\varepsilon} - \boldsymbol{\varepsilon}_p - \boldsymbol{\alpha}(\theta - \theta^i)\right]}_{\psi^e} \\ + \underbrace{c_0\left[\left(\theta - \theta^i\right) - \theta\, ln\left(\frac{\theta}{\theta^i}\right)\right] - \eta_0\theta + e_0}_{\psi^{th}} + \underbrace{\int_0^p R(p')\mathrm{d}p'}_{\psi^{vp}}.\end{aligned} \tag{50}$$

In the above potential, $\mathbb{C}_e$ denotes the elastic fourth order tensor, c_0 is the specific heat capacity per unit volume at constant pressure. Moreover, η_0 and e_0 are the initial entropy and the internal energy respectively. Finally, $R(p)$ is the hardening function related to the viscoplasticity, chosen here in the power law form

$$R\left(p\right) = Kp^n, \tag{51}$$

where K and n are hardening related material parameters. Following the classical procedure, derivatives of the Helmholtz free energy potential are used to identify the associated forces to the thermodynamic variables. Table 2 summarizes the various variables implicated to the thermodynamic description of the constitutive law. According to the second principle of thermodynamics, the dissipation is always positive or null. For this material, the mechanical and thermal dissipations are assumed decoupled and viscoplasticity is the only mechanism that stores energy permanently. From the usual thermodynamic arguments, the mechanical (local) dissipation is eventually

ACCEPTED MANUSCRIPT

Table 2: State and evolution laws

Observable state variables	Associated variables	
$\boldsymbol{\varepsilon}$	$\boldsymbol{\sigma} = \dfrac{\partial \psi}{\partial \boldsymbol{\varepsilon}} = \mathbb{C}_e : (\boldsymbol{\varepsilon} - \boldsymbol{\varepsilon}_p - \boldsymbol{\alpha}(\theta - \theta^i))$	
θ	$\eta = -\dfrac{\partial \psi}{\partial \theta} = \boldsymbol{\alpha} : \boldsymbol{\sigma} + c_0 \ln\left(\dfrac{\theta}{\theta^i}\right) + \eta_0$	
Internal state variables	**Associated variables**	**Evolution laws**
p	$R = \dfrac{\partial \psi}{\partial p} = R(p)$	$\dot{p} = -\dfrac{\partial F}{\partial R}\dot{\lambda} = \dot{\lambda}$
$\boldsymbol{\varepsilon}_p$	$-\boldsymbol{\sigma} = \dfrac{\partial \psi}{\partial \boldsymbol{\varepsilon}_p}$	$\dot{\boldsymbol{\varepsilon}}_p = \dfrac{\partial F}{\partial \boldsymbol{\sigma}}\dot{\lambda} = \dfrac{3}{2}\dfrac{\mathbf{dev}(\boldsymbol{\sigma})}{\mathrm{eq}(\boldsymbol{\sigma})}\dot{p}$

expressed as

$$\dot{\Phi} \;=\; \boldsymbol{\sigma} : \dot{\boldsymbol{\varepsilon}}_p - R\dot{p} \geq 0. \tag{52}$$

Moreover, the evolution laws for $\boldsymbol{\varepsilon}_p$ and p are obtained from a yield-type criterion

$$F(\boldsymbol{\sigma}, R) = \mathrm{eq}(\boldsymbol{\sigma}) - R - R_0, \tag{53}$$

through the classical normality rule. In the latter expression, $\mathrm{eq}(\boldsymbol{\sigma})$ denotes the von Mises equivalent stress and R_0 is the elasticity threshold. The evolution equations of the internal state variables are summarized in Table 2. Due to the viscoplastic nature of the material, the criterion F is not similar

ACCEPTED MANUSCRIPT

to the one used in plasticity, i.e. always negative or zero. Instead, it satisfies the following relation

$$\{ F \}_+ = Q(\dot{p}), \qquad Q(\dot{p}) = H\dot{p}^m, \tag{54}$$

where $\{ \bullet \}_+$ are the Macaulay brackets and H, m are viscous related material parameters.

The above constitutive law for thermoelastic-viscoplastic material is well established in the literature (Lemaitre and Chaboche, 1990). Its numerical implementation through a return mapping algorithm scheme (convex cutting plane) and the identification of its continuum tangent operators $\mathbb{D}^{\varepsilon}, \boldsymbol{D}^{\theta}, \boldsymbol{R}^{\varepsilon}$ and R^{θ} are discussed in detail in Chatzigeorgiou et al. (2016, 2018).

4. Multiscale FE^2 computation of fully coupled thermo-mechanical problem

To predict the macroscopic behavior of a composite structure while taking into account the effect of the microstructure and the thermo-mechanical couplings, a homogenization scheme within the framework of FE^2 technique has been implemented. The framework extends the approach developed in Tikarrouchine et al. (2018), by accounting the thermal part of the homogenization problem, as discussed in the previous section. At the macroscopic level the material is assumed as a homogenized medium subjected to appropriate thermo-mechanical boundary conditions. The response of any macroscopic point is obtained through the solution of a coupled thermo-mechanical microscopic problem, using periodic boundary conditions.

The algorithm of the two-scale finite element framework for the nonlinear thermo mechanical analysis, implemented in ABAQUS/Standard, is

ACCEPTED MANUSCRIPT

summarized in Figure 2. The computation of the thermo-mechanical tangent operators are described below:

Computation of thermo-mechanical tangent operators

The periodic boundary conditions in the unit cell can be numerically applied by using the concept of the constraint drivers. This technique introduces six constraint drivers as additional degrees of freedom that allow to apply any state of macroscopic stress, strain or even mixed stress/strain on a periodic finite element unit cell (see (Li, 1999; Shuguang and Anchana, 2004)). These degrees of freedom are linked to the unit cell through the kinematic equation $(20)_4$. The assigned displacement on these degrees of freedom represent macroscopic strains, as explained in detail in Tikarrouchine et al. (2018).

To obtain the thermo-mechanical tangent operators, seven loading cases are performed at the microscopic level (Figure 3). The microscopic tangent operators at every point of the unit cell obtained at the end of the stress field computations are utilized in these analyses and they are considered constant. At first, six mechanical-type loading cases are carried out, in which elementary strain states (one component equal to 1 and the rest zero) are assigned at the constraint drivers. In each loading case, the forces generated at the constraint drivers divided by the volume represent a column of the macroscopic tangent operator $\overline{\mathbb{D}}^{\varepsilon}$ (Tikarrouchine et al., 2018), while the strains at every microscopic point represent a column of the concentration tensor $\mathbb{A}^{\varepsilon}$. Assembling the results of the six mechanical cases and using the formula (48_3), the macroscopic operators $\overline{\mathbb{D}}^{\varepsilon}$ and $\overline{\boldsymbol{R}}^{\varepsilon}$ are obtained. In the seventh thermal-type loading case, zero displacement is considered at the

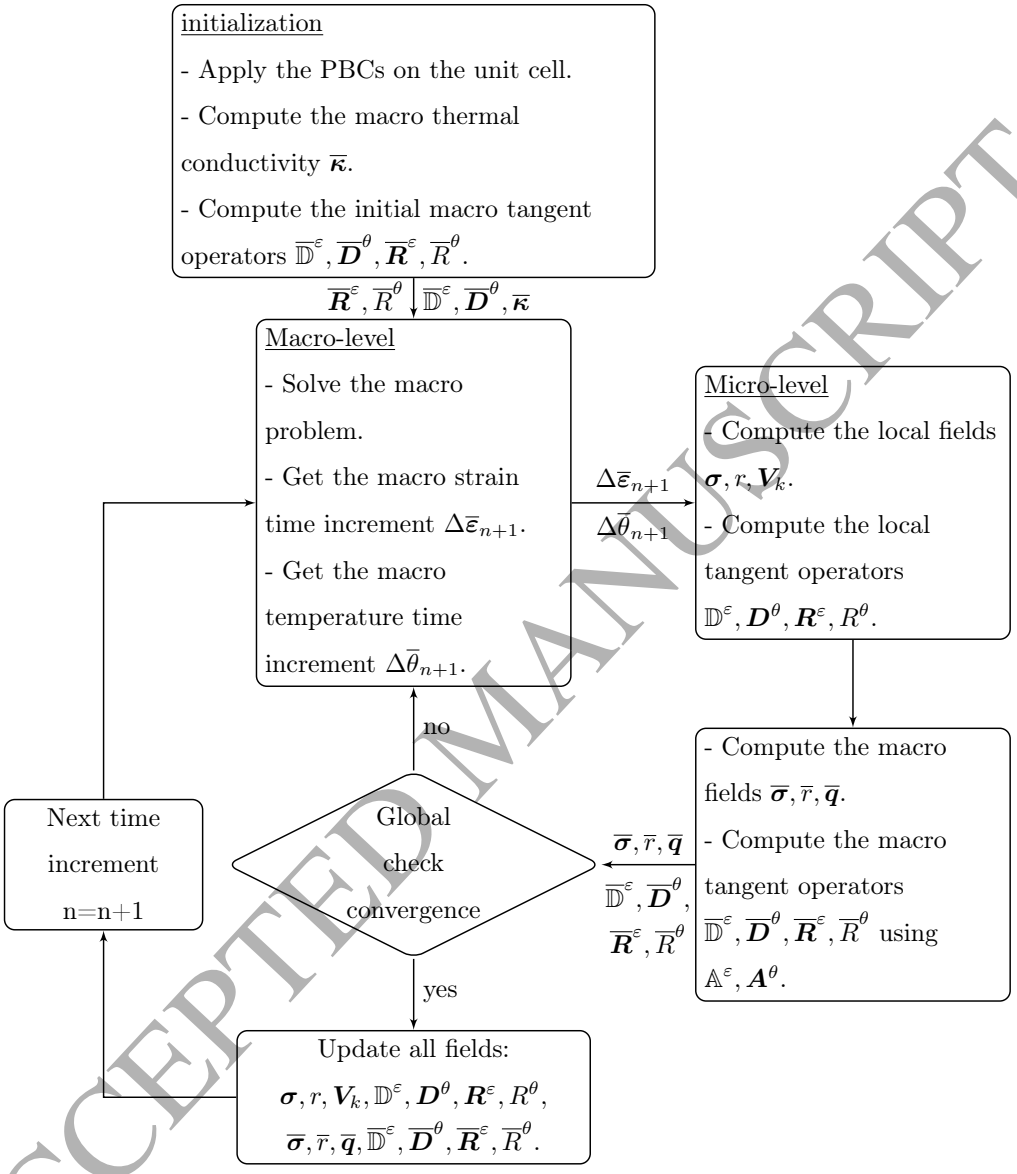

Figure 2: The flow chart of the two scales FE^2 algorithm for the non-linear fully coupled thermo-mechanical response of composite in ABAQUS/Standard.

ACCEPTED MANUSCRIPT

constraint drivers, while a temperature $\overline{\theta} = 1$ is assigned at every microscopic point. The forces generated at the constraint drivers divided by the volume represent the macroscopic tangent operator $\overline{\boldsymbol{D}}^{\theta}$, while the strains at every microscopic point represent the concentration tensor $\boldsymbol{A}^{\theta}$. The last thermo-mechanical tangent operator $\overline{R}^{\theta}$ is obtained by the volume averaging formula of equation $(48)_4$.

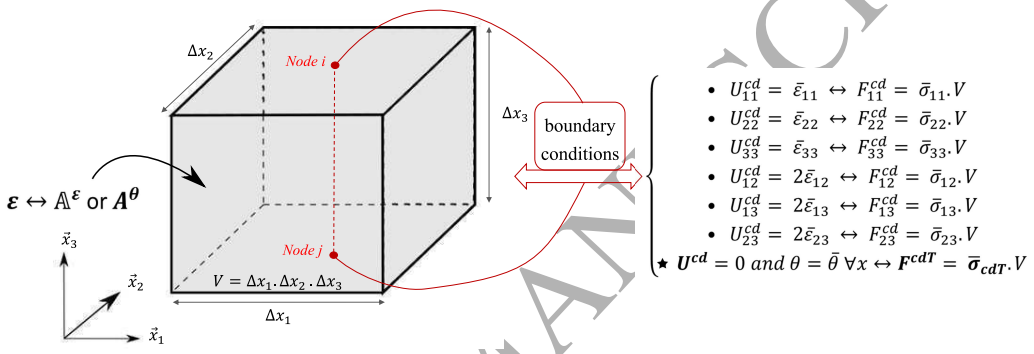

Figure 3: Connection of the constraint drivers with the unit cell.

Calculation of the macroscopic thermal conductivity

As described in the previous section, the macroscopic thermal conductivity $\overline{\boldsymbol{\kappa}}$ is computed once through the periodic homogenization procedure separately from the microscopic equilibrium. In that sense, it can be seen as a separate calculation from the iterative FE^2 procedure. In the finite element analysis for periodic media the unit cell is associated with periodic mesh. This implies that, for each border node, there is always another node at the same relative position on the opposite side of the unit cell. Applying the macroscopic temperature gradient $\overline{\boldsymbol{\nabla}\theta}$ on the unit cell, the temperature fields for each pair of opposite parallel border nodes (denoted by the indices

i and j), follow the general relationship (Suquet, 1983):

$$\theta_i - \theta_j = \overline{\boldsymbol{\nabla}\theta} \cdot (\boldsymbol{x}_i - \boldsymbol{x}_j)\,. \tag{55}$$

From a computational point of view, with the help of the concept of the

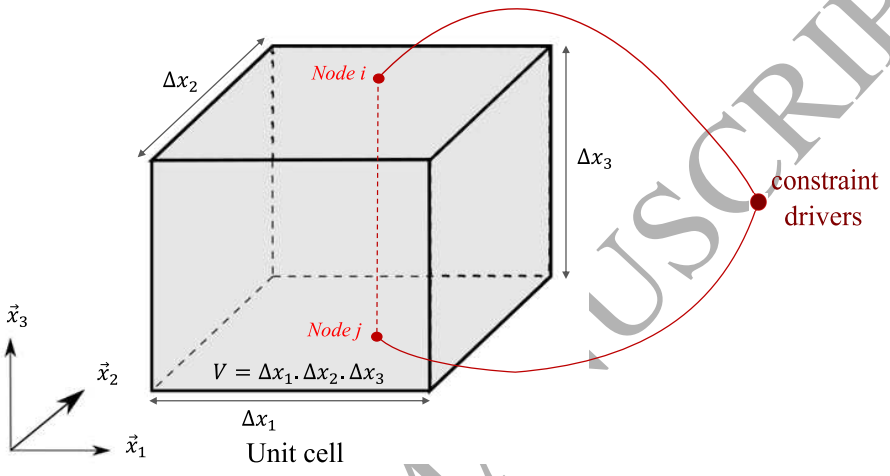

Figure 4: Opposite side of a unit cell are connected with constraint drivers.

constraint drivers, one can apply numerically the three components of the macroscopic temperature gradient vector $\overline{\boldsymbol{\nabla}\theta}$ on the unit cell, taking into account the periodic boundary conditions (see Figure 4). More detailed exposition about this concept is given in Li (1999, 2000); Shuguang and Anchana (2004). These constraint drivers (three additional nodes) are linked to the mesh of the unit cell through equation 55. In the finite element calculations in ABAQUS/Standard, the heat transfer analysis computes a heat flux vector on the additional nodes that corresponds to the macroscopic heat flux $\overline{\boldsymbol{q}}$ multiplied by the volume V of the unit cell on the additional nodes. Applying the three macroscopic temperature gradients

$$\overline{\boldsymbol{\nabla}\theta}^1 = (1 \;\; 0 \;\; 0)^T\,, \quad \overline{\boldsymbol{\nabla}\theta}^2 = (0 \;\; 1 \;\; 0)^T\,, \quad \overline{\boldsymbol{\nabla}\theta}^3 = (0 \;\; 0 \;\; 1)^T\,, \tag{56}$$

ACCEPTED MANUSCRIPT

the generated macroscopic heat fluxes $\overline{\boldsymbol{q}}^1$, $\overline{\boldsymbol{q}}^2$ and $\overline{\boldsymbol{q}}^3$ correspond to the three columns of the macroscopic thermal conductivity tensor:

$$(\overline{\boldsymbol{\kappa}})_{ij} = (\overline{\boldsymbol{q}}^i)_j. \tag{57}$$

5. Applications and Capabilities of the FE^2 framework

The proposed two-scale finite element framework presented in section 4 is applied considering thermoelastic-viscoplastic matrix, described in subsection 3.3, and thermoelastic reinforcement.

The main purpose of this section is to demonstrate the performance and the capabilities of the thermo-mechanically, fully coupled two-scale finite element technique to predict the overall response of 3D composite structures facing complex cases of thermo-mechanical loading. The section is partitioned into three parts to highlight the different aspects of the proposed technique. The first part 5.1 present the validation of the multi-scale approach by comparing the numerical results with that of the fully meshed Finite Element (FE) model under adiabatic conditions. Therefore, a microstructure with a spherical inclusion is considered under a given macroscopic load. In the second part 5.2.1, a tensile test on 3D non-symmetric notched plate is studied under three different displacement rates with Robin boundary conditions that are applied in two different surfaces. Finally, the third part 5.2.2 corresponds to cyclic loading (tensile-compression) on the same non-symmetric notched plate under varying thermal conditions. It should be noted that in the last two examples, the composite material is considered as a thermoelastic-viscoplastic matrix reinforced by thermoelastic aligned short glass fibers.

ACCEPTED MANUSCRIPT

5.1. Validation of FE^2 approach by comparison with full structure

In order to validate the proposed approach presented previously, the numerical results are compared with that of a single scale FE computation, considering a full structure of $10 \times 10 \times 10$ unit cells (Figure 6) under the same boundary conditions. For the two numerical simulations, a 3D composite cube under displacement controlled loading in direction 11 (up to 10% with a rate of 1% per s) and zero Neumann thermal boundary conditions is simulated. The descritization of the FE^2 for the macroscopic model and for the unit cell at each macroscopic point is shown in figure 5. The coarse discretisation of the macroscopic model consists of 64 nodes and 27 elements of type C3D8T (8 node with 8 integration points, 3D solid elements for coupled temperature displacement analysis). Furthermore, the unit cell discretization is performed using 292 nodes and 1219 C3D4 elements[1] (Figure 5b). The unit cell consists of thermoelastic-viscoplastic matrix reinforced by thermoelastic spherical inclusion. On the other hand, the full structure consists of the same unit cell, repeated periodically in the three spatial directions (Figures 6a and 6b). Its discretization is performed with C3D4T elements (4 nodes tetrahedral elements with one integration point, 3D solid elements for coupled temperature displacement analysis). The coarse discretization involves 208651 nodes and 1219000 elements (Figure 6). The volume fractions of the matrix and the fibers are $V^m = 0.8$ and $V^f = 0.2$ respectively for the two

[1]From the microscopic analysis only the coupled thermo-mechanical terms are required. These can be computed directly from the stress, the strain, the temperature and the internal variables through the mechanical constitutive law. Thus, there is no need to utilize thermomechanically coupled finite elements at this scale.

models.

The two cases (FE^2 and full structure) are subjected to the same thermo-mechanical loading conditions. The material parameters of the two phases are presented in Tab 3. For the macroscopic thermal conductivity $\overline{\boldsymbol{\kappa}}$, it is found from the solution of the purely thermal problem (presented in section 4) that $\overline{\boldsymbol{\kappa}}$ is isotropic, with $\overline{\kappa}_{11} = \overline{\kappa}_{22} = \overline{\kappa}_{33} = 4.23\,10^{-4}$ W/mmK. Figure 7 illus-

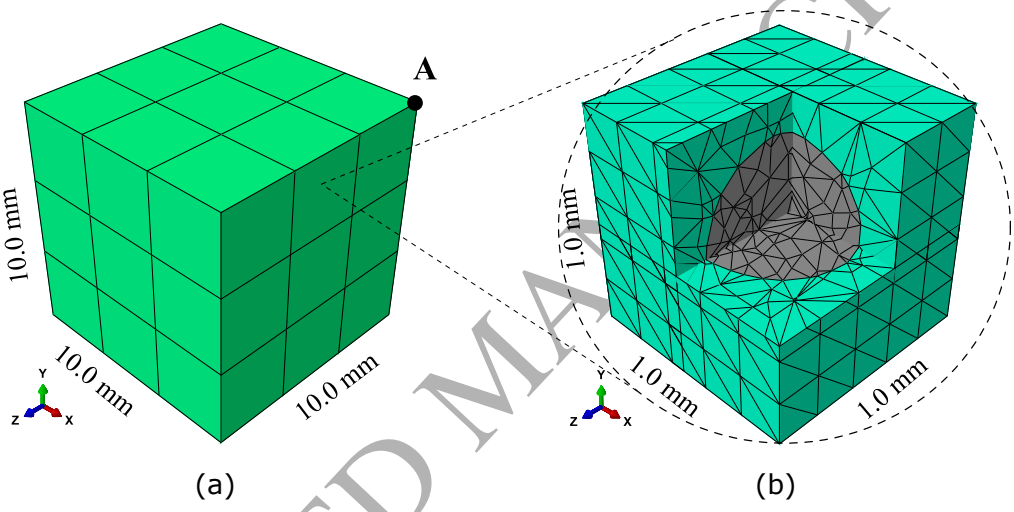

Figure 5: Coarse FE discretization of (a) the macroscopic model and (b) the microstructure observed at each macroscopic integration point of the FE^2 simulation.

trates the macroscopic response on the whole volume of the FE^2 model as well as for full structure in terms of stress-strain in the direction 11. The results of the two approaches show a very good agreement between the two analyses, demonstrating the accuracy and the capability of the proposed FE^2 method to predict the overall response of 3D non-linear multi-scale composite structures. A similar validation can be found in (Drago and Pindera, 2007) for 2D problems. The relative error plot $\left(\left[||\overline{\sigma}_{11}^{\mathrm{FE}^2}|| - ||\overline{\sigma}_{11}^{\text{Fully meshed}}||\right] / ||\overline{\sigma}_{11}^{\mathrm{FE}^2}||\right)$ con-

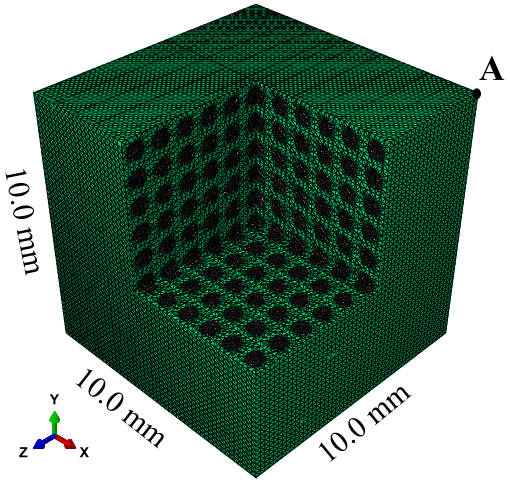

(a) Dimensions and Coarse FE discretization of fully structure.

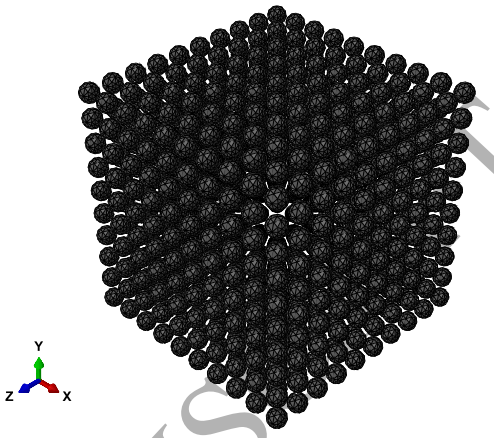

(b) Coarse FE discretization of the inclusions.

Figure 6: Coarse FE discretization of the 3D fully structure.

firms the good agreement of the two simulations. The multi-scale solution, compared to the full structure solution, presents a relative error between 0 and 0.3% (Figure 8). Figure 9 presents the macroscopic temperature difference between the two approaches in the point A situated in the same position in the two structure. It must be noted that a numerical artifact of temperature elevation can be observed at the beginning of both FE^2 and single scale FE analyses. This non-physical temperature rise is due to the choice of the large time step for reducing the computational time. In addition, one can also observe that in the thermal response the maximum difference between the two computations is 0.25 K, which is acceptable for such complex analysis.

ACCEPTED MANUSCRIPT

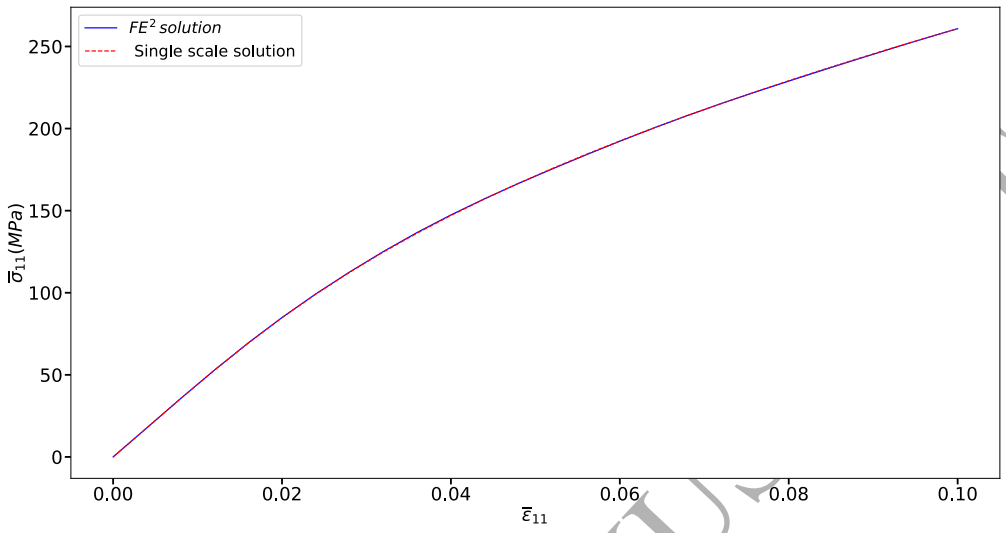

Figure 7: Comparison of the overall response of the FE^2 and single scale FE solutions in terms of $\overline{\sigma}_{11}$ Vs $\overline{\varepsilon}_{11}$.

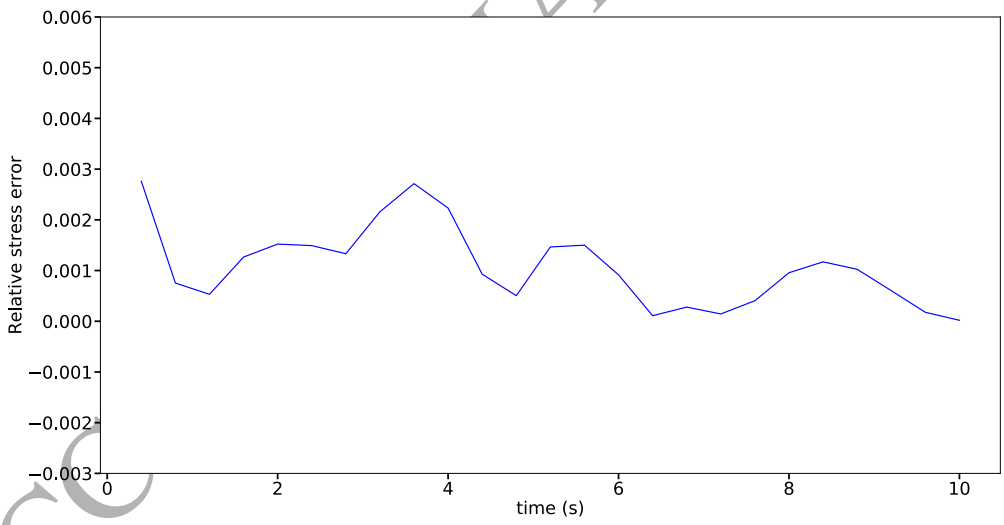

Figure 8: Relative stress error of the macroscopic stress response of the FE^2 and single scale FE solutions.

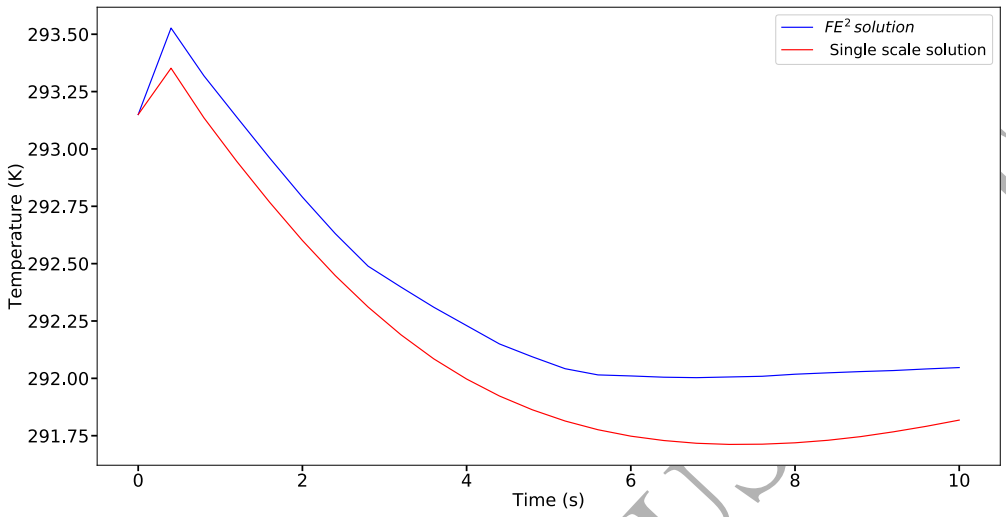

Figure 9: Comparison of the macroscopic temperature of the two approaches in point A situated in the same position in the two structures.

5.2. 3D non-symmetric notched plate with short fiber reinforced composite

In order to demonstrate the approach capabilities in simulating the overall behavior of 3D composite structures, the present section deals with two examples of FE^2 analysis performed on 3D non-symmetric structure (Figure 10) made of polymer matrix reinforced with aligned glass short fibers arranged in a periodic hexagonal array (Figure 11). Figure 10 presents the dimensions of the macroscopic structure as well as the coarse FE discretization that consists of 84 elements of type C3D8T. In the two examples the 3D structure is subjected to a complex thermo-mechanical loading path. The scope is to illustrate the ability of the technique to i) capture the rate effects due to changes of the loading rate and ii) compute the dissipation at different positions in the structure due to the cyclic loading.

The microstructure that represents every macroscopic point of the struc-

ACCEPTED MANUSCRIPT

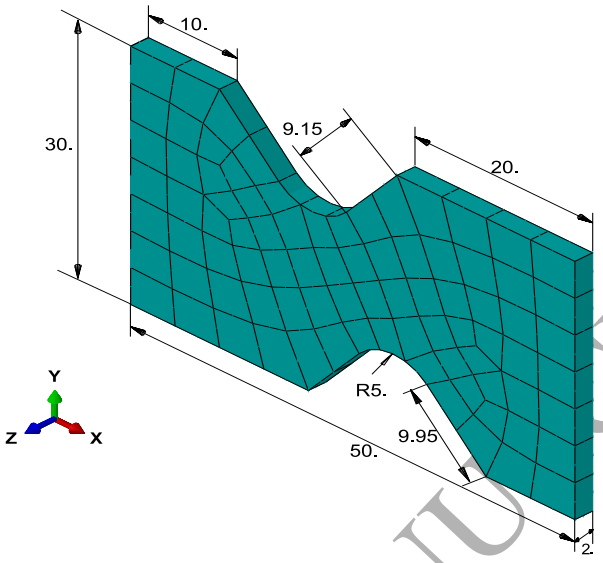

Figure 10: Dimensions and a coarse discretisation of the macroscopic 3D non-symmetric notched plate.

ture presented in Figure 11 is meshed using 5881 elements of type C3D4 (4 node with one integration point). The volume fractions of the matrix and the fibers are $V^m = 0.844$ and $V^f = 0.156$ respectively. The aspect ratio for the elliptic fibers is (4.5, 1, 1). The material properties for the thermoelastic fibers and the thermoelastic-viscoplastic polymer matrix are listed in Tab. 3.

As it is discussed in the previous sections, the macroscopic thermal conductivity is computed once, separately from the FE^2 analysis. From the solution of the purely thermal problem presented in section 4, it is found that the macroscopic thermal conductivity (Eq. 57) presents transverse isotropy for the short fibers reinforced composite, with x as the axis of symmetry. The solution of the heat transfer analysis performed in ABAQUS is pre-

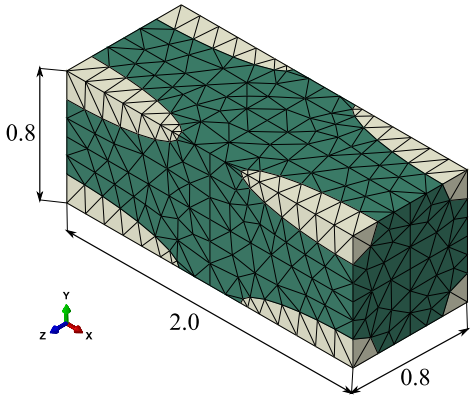

(a) Composite microstructure. The gray domain represents glass fibers and the green domain represents the polymer matrix.

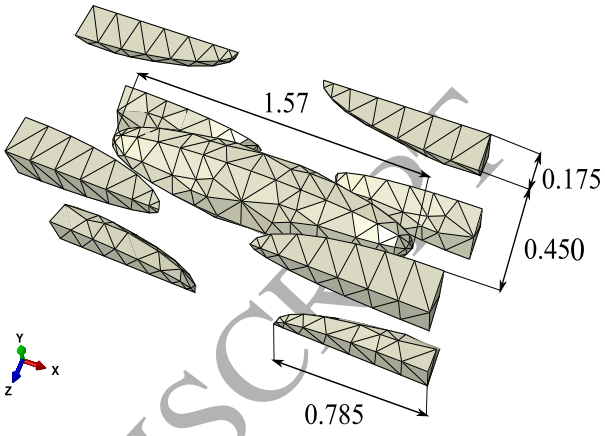

(b) Dimensions and the spacial arrangement of the short glass fibers.

Figure 11: Discretisation of the short fiber reinforced composite unit cell with tetrahedral elements type C3D4 as well as the spacial dimensions.

sented in Figure 12 for the three components of the macroscopic thermal conductivity vector $\overline{\boldsymbol{\kappa}}$. The computations yield that $\overline{\kappa}_{11} = 4.28\,10^{-4}$ and $\overline{\kappa}_{22} = \overline{\kappa}_{33} = 4.02\,10^{-4}$ W/mmK.

5.2.1. Strain rate controlled thermo-mechanical loading

In this example, the overall response of the 3D composite structure is predicted through the proposed fully coupled thermo-mechanical FE^2 technique and the results highlight the effect of the loading rate on the stress-strain response, caused by the viscous behavior of the polymer matrix. Figure 13a presents the macroscopic thermo-mechanical boundary conditions applied on the structure. The structure is clamped on the left side and subjected to the mechanical loading path of Figure 13b at the right side. The simulation is

ACCEPTED MANUSCRIPT

ACCEPTED MANUSCRIPT

Table 3: Material parameters for the analyzed composite, consisting of short fiber reinforced thermo-viscoplastic polymer matrix

Parameter	Matrix	fiber	unit
Young modulus E^m	2.680	72.0	GPa
Poisson ratio ν^m	0.3	0.26	-
thermal expansion α	95.e-06	9.0e-06	1/K
density ρ	1.19e-03	2.53e-03	g/mm^3
specific heat capacity C_p	1590	830	J/gK
thermal conductivity κ	0.35e-03	0.93e-03	W/mmK
elastic limit R_0	15	–	MPa
K	365.0	–	MPa
n	0.39	–	-
H	180.0	–	MPa.s^m
m	0.3	–	-
θ_{int}	293.15	293.15	K

carried out considering Robin type thermal boundary conditions. In Figure 13a, $\overline{q}_i$ is the heat flux across the surface, h_{ci} is the film coefficient of the fluid surrounding the structure. $\overline{\theta}$ and $\overline{\theta}_0$ are the temperature at a point in the surface and a reference sink temperature value respectively. The displacement controlled path consists in two loading steps with different velocities ($\dot{\overline{u}}_x^{(1)} = 2.0\,10^{-2}\,mm.s^{-1}$ and $\dot{\overline{u}}_x^{(2)} = 2.0\,10^{-3}\,mm.s^{-1}$) followed by an unloading stage at a displacement rate of $\dot{\overline{u}}_x^{(3)} = 2.2\,10^{-2}\,mm.s^{-1}$. In the first step, the displacement u is increased linearly from 0 to $2\,mm$ in $100s$. In the second step, the loading rate is decreased and the displacement is increased

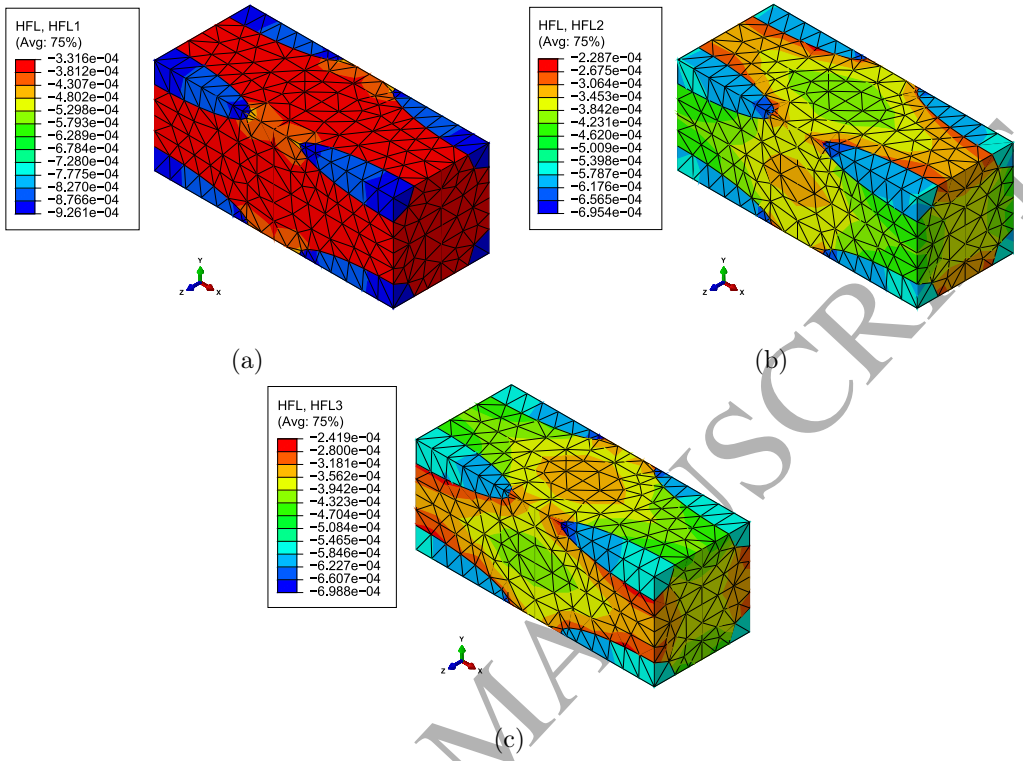

Figure 12: Fields generated for the calculation of the macroscopic thermal conductivity $\overline{\kappa}$ in three directions: (a) $\overline{\kappa}_{11}$, (b) $\overline{\kappa}_{22}$ and (c) $\overline{\kappa}_{33}$.

linearly from 2 to 2.2 mm in 100s. After 200s, the applied displacement decrease from 2.2 to 0 mm in 100s. A constant time increment $\Delta t = 5s$ is imposed throughout the whole analysis. The film condition is applied on the front surface with film coefficient h_{c1} and the top surface with film coefficient h_{c2}, as depicted in Figure 13b. The two film coefficients are equal to $h_{c1} = 2.10^{-4}\, W/mm^2K$ and $h_{c2} = 6.10^{-4}\, W/mm^2K$ respectively and are assumed to remain constant during the analysis. In this simulation, the initial temperature of the structure is $\overline{\theta}_{int}$ = 293.15 K (20^{o}C) and the sink temperature is $\overline{\theta}_0$ = 310.15 K (37^{o}C). In the thermo-mechanical simulation,

the temperature $\overline{\theta}_{int}$ must be equal to θ^i of equation 49 to avoid the residual stresses and to ensure that the initial state of the unloaded structure is in thermal equilibrium.

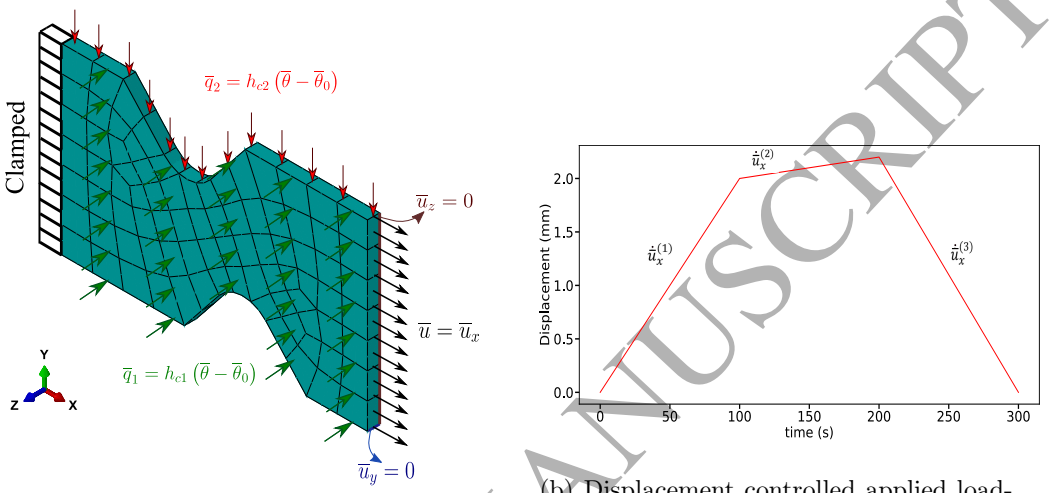

(a) Thermo-mechanical boundaries conditions on the 3D composite structure.

(b) Displacement controlled applied loading $\overline{u}_x$ path with several displacement rates.

Figure 13: Applied thermo-mechanical boundary conditions and the mechanical loading path on the macroscopic structure.

The obtained results of the analysis are demonstrated at characteristic macroscopic points of the structure. The Figures 14 and 15 present the macroscopic and microscopic stress fields in the direction 11 at $t = 200s$ and $t = 300s$. As expected, it can be clearly seen that the major part of the stress in the direction of the mechanical loading is transferred to the fibers. Figure 16 shows the stress-strain curves at the macroscopic characteristic critical point A of the structure (Figure 14) at the end of the thermo-mechanical loading. The results illustrate also that the response of the composite is highly influenced by the presence of the matrix through the relaxation phe-

ACCEPTED MANUSCRIPT

ACCEPTED MANUSCRIPT

nomena. On the other hand, the temperature response exhibits an elevation of 16°C, which is mainly due to the thermal conditions (convection), as presented in Figures 17 and 18 for analysis times of $t = 100s, t = 200s$ and $t = 300s$. This elevation of the macroscopic temperature, demonstrated by the FE^2 computations, can have an important impact behavior of the thermoplastic due to its low thermal conductivity.

The interest of the FE^2 approach resides also in the estimation of the local and global dissipation. Figure 19 presents the local dissipation distribution $\dot{\phi}$ in the microstructure at the critical point A for analysis times of $t = 100s$ and $t = 300s$. It can be clearly observed that the dissipation is localized in the interface fiber-matrix and especially at the fibers end. In Figure 20 the evolution of the macroscopic local dissipation $\overline{\dot{\Phi}}$ according to the time is presented in several characteristic points of the structure (A, B, C, D, E and F). It has a rapid increase when the composite enters in the plastic regime, followed by a sudden drop and a long small decrease during the relaxation and the unloading steps. Finally, a short increase during the compression is obtained when the composite enters in the final stage of plastification close to the end of the analysis.

5.2.2. Cyclic thermo-mechanical loading

The third numerical example presents a practical design application of composite structures that requires the numerical study of the response under cyclic loading. The structure is clamped at the left side and subjected to the cyclic loading of Figure 21b on the right side (tensile-compression test).

In the first steps (from $t = 0s$ to $t = 800s$), the front and the top surfaces of the structure is the Robin boundary on which a forced convection

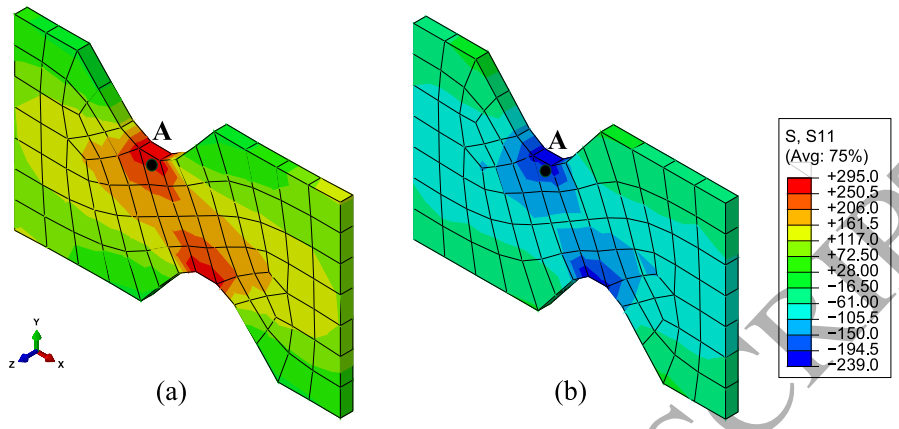

Figure 14: Macroscopic stress field distribution in directions 11 (in MPa) using FE^2 solution for analysis time of (a) t=200s and (b) t=300s.

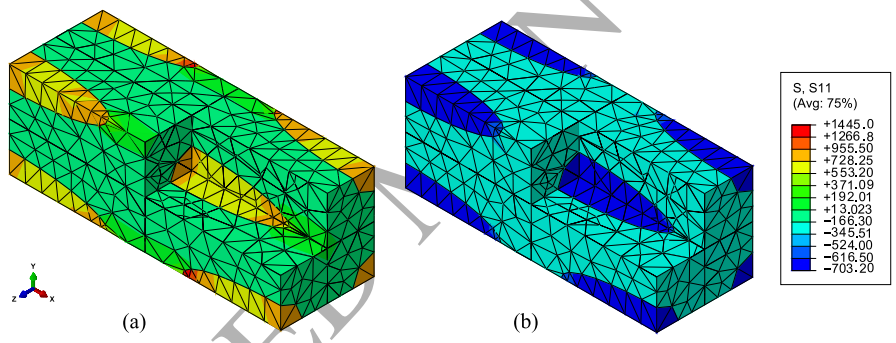

Figure 15: Microscopic stress field distribution in directions 11 (in MPa) at critical point A of the structure using FE^2 solution for analysis time of (a) t=200 s and (b) t=300s.

heat transfer is modelled. Two different film coefficients on the two different surfaces, as depicted in Figure 21a, are imposed. The film coefficient of the front surface is assumed to be $h_{c1} = 4.10^{-4}\, W/mm^2K$, while the second one on the top surface is assumed to be $h_{c2} = 8.10^{-4}\, W/mm^2K$. The other step of simulation (from $t = 800s$ to $t = 1000s$) is carried out with zero Neumann boundary condition. The external temperature is assumed to be

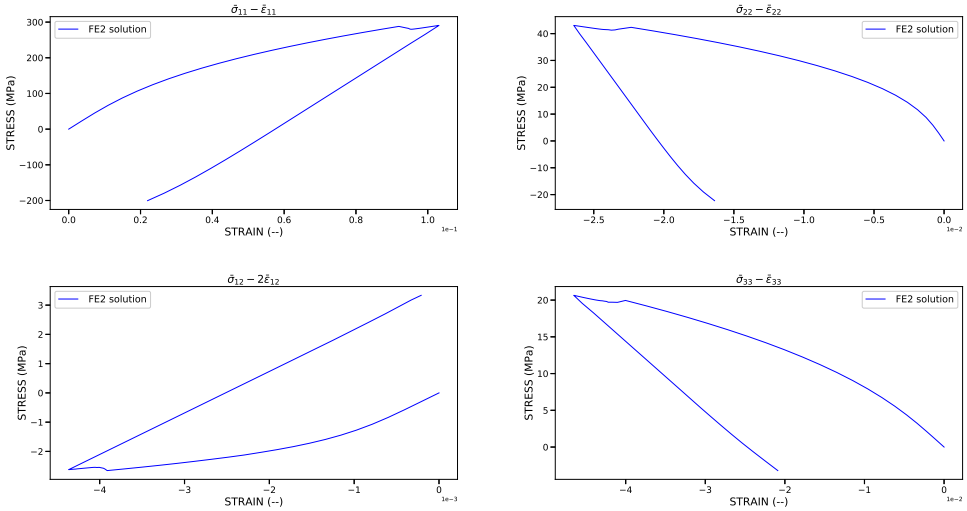

Figure 16: Evolution of the macroscopic stress as a function of the strain at the critical point A of the structure Figure 14 in the directions 11, 22, 33 and shear 12.

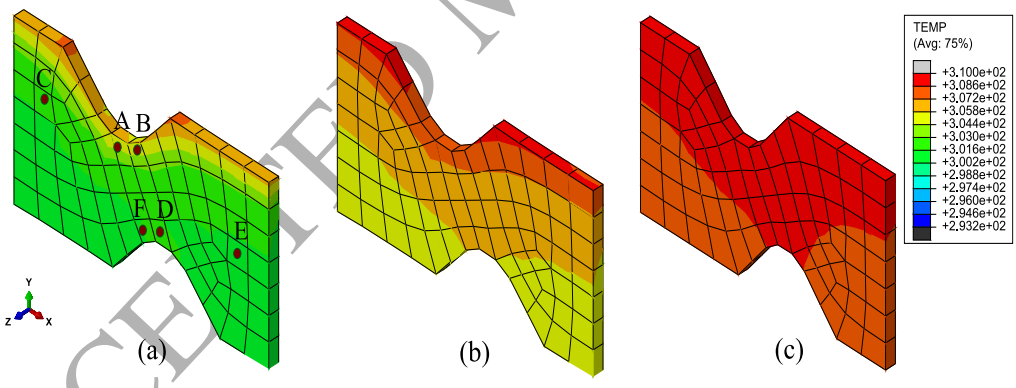

Figure 17: Macroscopic spatio-temporal temperature distribution (in K) in the composite structure for analysis time of (a) t=100s, (b) t=200s and (c) t= 300s. The heterogeneous temperature field tends to be uniform by the end of the analysis.

ACCEPTED MANUSCRIPT

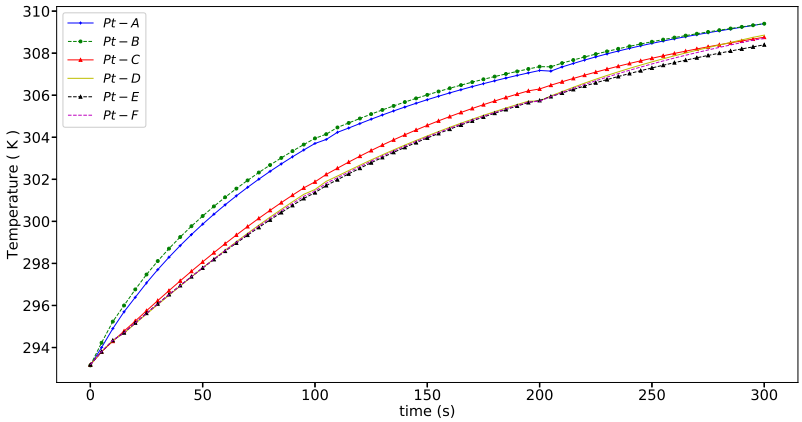

Figure 18: Evolution of the macroscopic temperature at the characteristic points (A, B, C, D, E and F) for the total analysis time. An overall temperature elevation of 16°C is obtained during the thermomechanical loading of 300s.

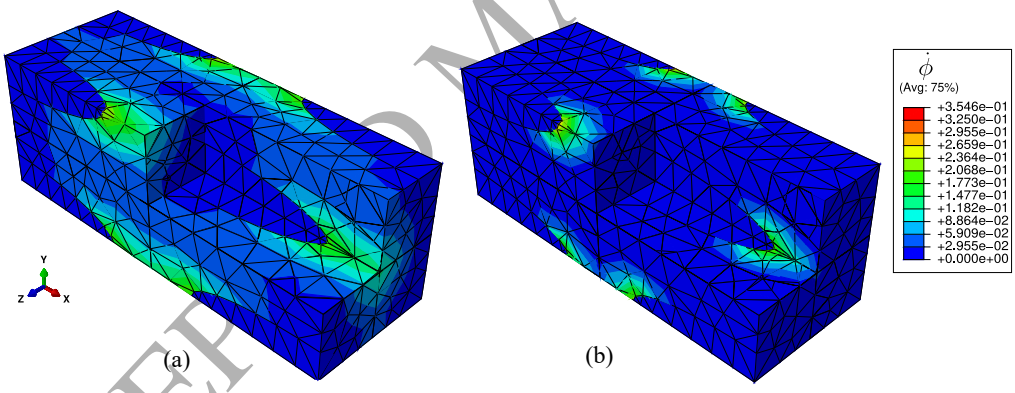

Figure 19: Local dissipation distribution field $\dot{\Phi}$ in the microstructure corresponding to the characteristic critical point A of the structure for analysis time of (a) t=100s and (b) t= 300s (in $mW.mm^{-3}$).

$\overline{\theta}_0 = 313.15$ K (40^oC). It should be mentioned that, for this example, the value of the specific heat capacity has been artificially increased 1000 times.

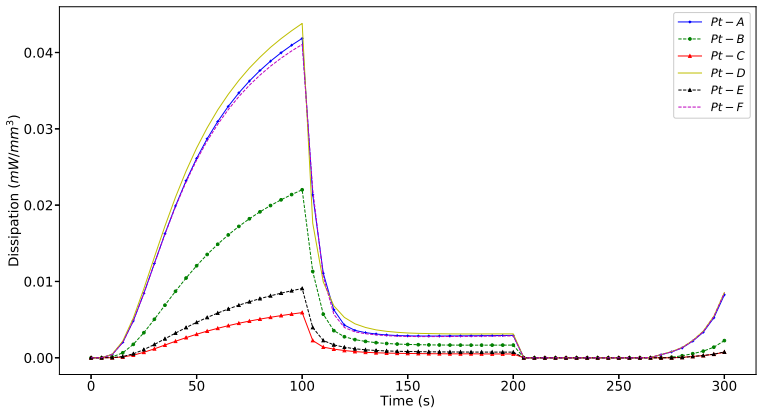

Figure 20: Evolution of the macroscopic local dissipation $\overline{\dot{\Phi}}$ at the characteristic points (A, B, C, D, E and F) during the analysis.

This non-physical choice of value has been adopted to avoid some technical problems encountered during the process computation using the thermomechanical solver of the FE software ABAQUS. Up to the authors knowledge, these technical issues aborting the calculations are related to certain units consistency in the ABAQUS solver. Nevertheless, this point does not alter the goal of this example, which consists in demonstrating the capability of the FE^2 computations to simulate cyclic loading.

The stress fields, the macroscopic temperature and the evolution of dissipation are presented at characteristic points of the structure. In the Figures 22 and 23, the macroscopic and the microscopic stress fields in direction 11 are presented for two analysis times that correspond to tensile (Figures 22a and 23a) and compression (Figures 22b and 23b) conditions respectively. As expected, the major part of the stress is transferred to the fibers and the interface between fibers and matrix. Figures 24 show the macroscopic stress

ACCEPTED MANUSCRIPT

evolution due to cyclic loading at the critical point A of the structure in three directions (11, 22, 33 and shear 12). It is clear that the higher amplitude of stress is in the fibers direction. The material exhibits an accumulation of strain from one cycle to another. In addition, hysteresis loops can also be observed at each cycle due to the nature of the polymer matrix. Figure 25 presents the macroscopic temperature evolution due to the cyclic loading and forced convection at different time steps. As expected, the temperature elevation induced by the dissipative mechanisms and the forced convection remains relatively low (about 1 to 4 ^{o}C, Figure 26). Between 0 and 800s the macroscopic temperature presents an almost linear elevation, while at later times the temperature is constant with a slight decrease. The temperature elevation is mainly caused by the forced convection and is not significantly influenced by dissipation, due to low number of cycles (3 - 5 cycles). At low cycle loading the heating due to the dissipation is negligible, while for high number of cycles (100 - 1000 cycles) the accumulation of dissipation is expected to be significant and the relative increase of temperature easier observable. From an energetic point of view, the spatial distribution of the dissipation is presented in Figure 27 at the critical point A for three time steps, $t = 400s, t = 600s$ and $t = 800s$. It is worth noticing that, using the energy balance equation, one can estimate the effect of the dissipation on the temperature rate. Indeed, the macroscopic heat equation reads

$$\overline{\rho C_p}\ \dot{\overline{\theta}} = -\overline{\mathbf{div}}(\overline{\boldsymbol{q}}) + \text{thermomechanical terms} + \dot{\overline{\Phi}}. \tag{58}$$

Figure 28 shows the temporal variation of the dissipation $\dot{\overline{\Phi}}$ divided by the $\overline{\rho C_p} =< \rho C_p >$ for different points of the structure during tension and compression. As mentioned before, the heat generated by the dissipation appears

to be small due to the low number of simulated cycles. Unfortunately, high number of cycles, considering the full thermo-mechanical coupling in multi-scale FE^2 techniques, cannot be simulated easily, due to the computational cost.

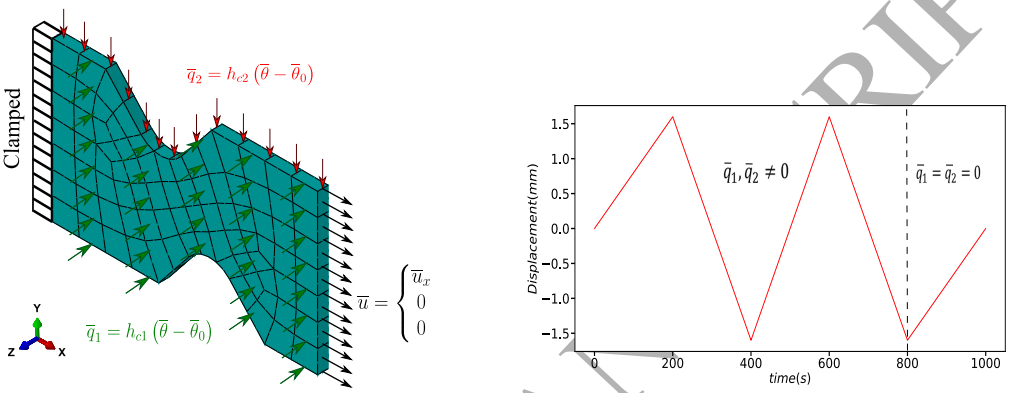

(a) Coarse FE discretisation and the thermo-mechanical boundaries conditions on the macroscopic composite structure.

(b) Mechanical cyclic loading path.

Figure 21: Coarse FE discretisation of the 3D structure and the applied thermo-mechanical boundary conditions.

ACCEPTED MANUSCRIPT

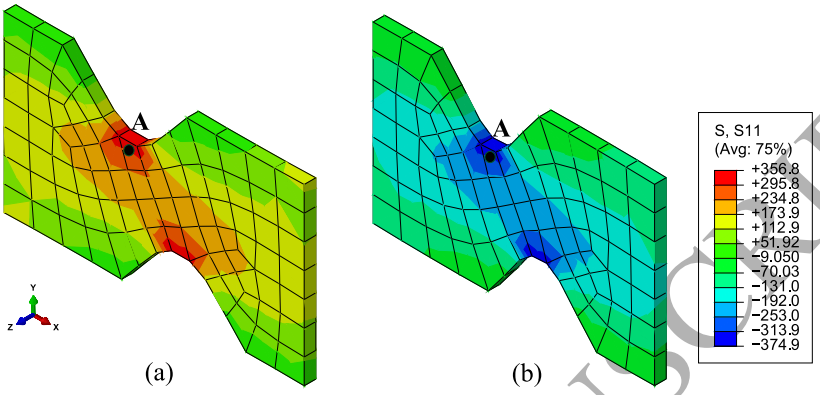

Figure 22: Macroscopic stress field of the composite structure in direction 11 for analysis time of (a) t=600s that correspond to the tensile and (b) t=800s that correspond to the compression.

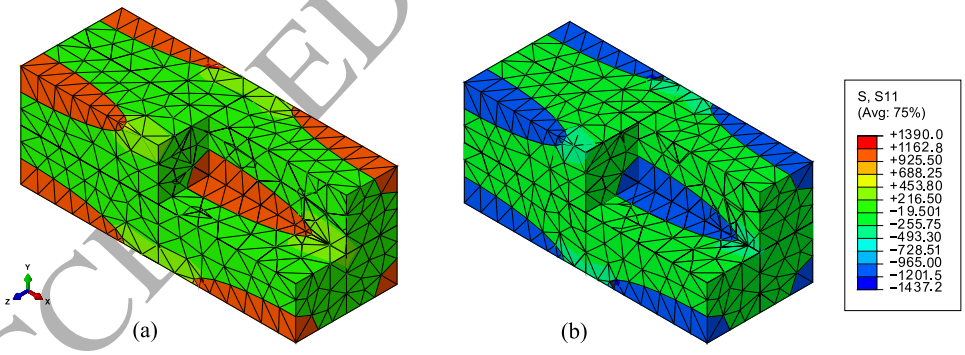

Figure 23: Microscopic stress field of the microstructure that correspond to the critical point A of the structure in direction 11 for analysis time of (a) t=600s that correspond to the tensile and (b) t=800s that correspond to the compression.

ACCEPTED MANUSCRIPT

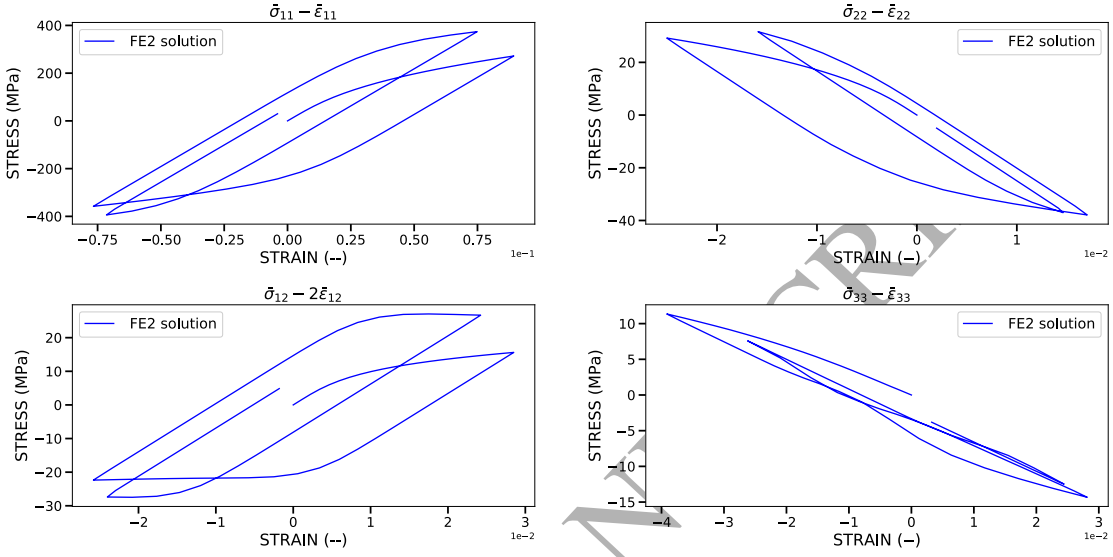

Figure 24: Evolution of the macroscopic stresses with strain at the critical point A of the structure Figure 22 in the directions 11, 22, 33 and shear 12.

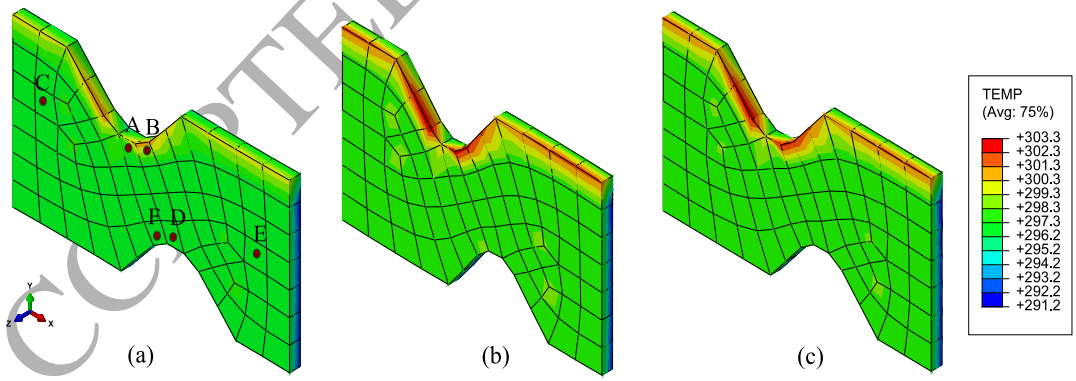

Figure 25: Macroscopic temperature distribution (in K) in the structure for analysis time of (a) t=600s, (b) t=800s and (c) t=1000s.

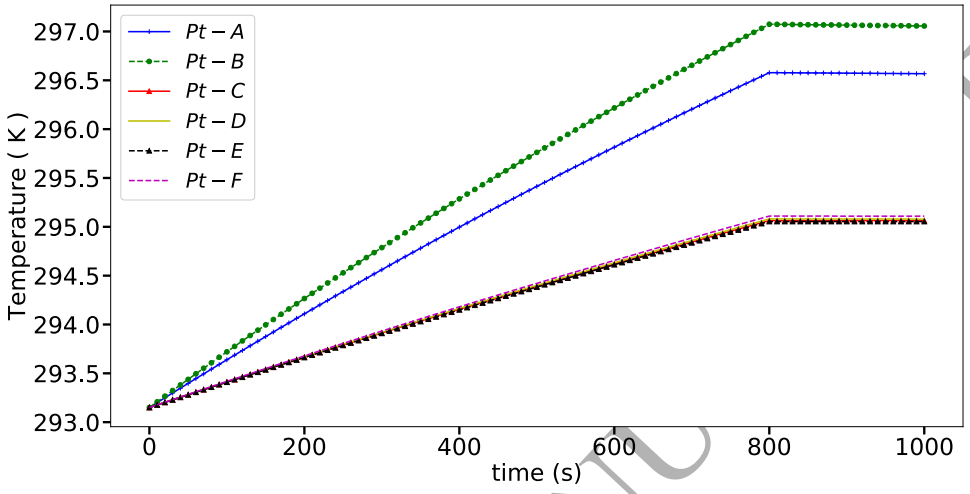

Figure 26: Evolution of the macroscopic temperature at the characteristic points (A, B, C, D, E and F) for the total analysis time.

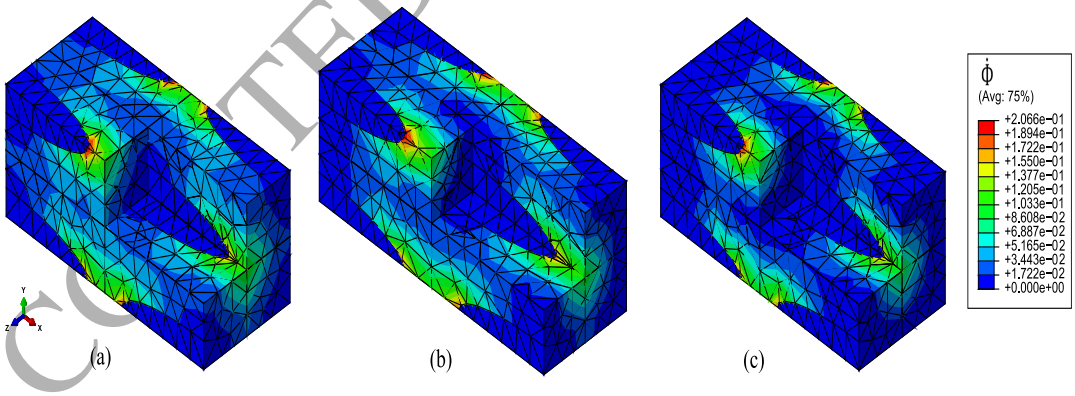

Figure 27: Local dissipation field (in $mW.mm^{-3}$) in the critical point A of the structure for analysis time of (a) t=400s, (b) t=600s and (c) t=800s.

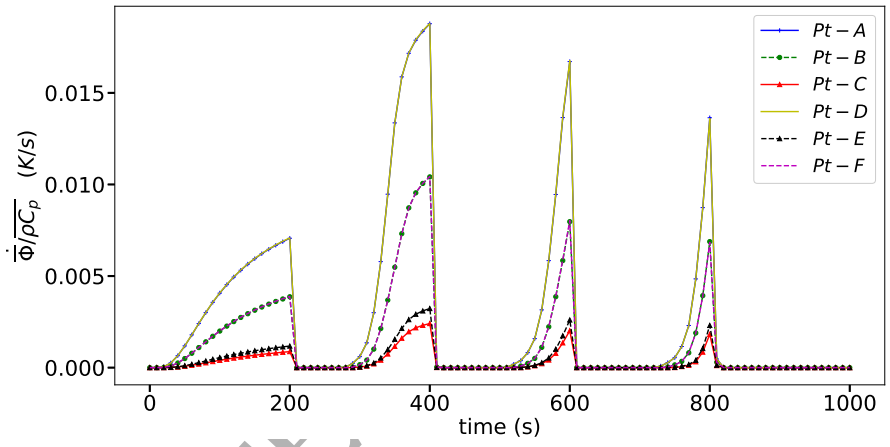

Figure 28: Evolution of the local dissipation effect on the macroscopic temperature at the characteristic points (A, B, C, D, E and F) during the analysis.

ACCEPTED MANUSCRIPT

ACCEPTED MANUSCRIPT

6. Conclusions and further work

This work presents a multi-scale three-dimensional fully coupled thermo-mechanical modelling strategy for composite structures, considering non-linear material response and using the FE^2 framework. The approach is fully integrated in the finite element commercial code ABAQUS/Standard, using parallel computations. An established framework restricted to mechanical loading (Tikarrouchine et al., 2018) is extended to fully coupled thermo-mechanical homogenization scheme to predict the thermo-inelastic structural response considering small deformations and rotations. The main advantage of the developed simulation technique resides in its ability to integrate any kind of 3D periodic microstucture with any type of thermo-mechanical non-linear constitutive model for the constituents (thermoplastic, thermo-viscoelastic, thermoelastic-viscoplastic). The numerical applications performed in this article focus on the thermoelastic - viscoplastic regime and the obtained results capture the rate-dependency in the structural behavior and the thermo-mechanical couplings in the polymer composites under complex thermo-mechanical loading.

The proposed strategy has been validated through a comparison with equivalent single scale simulations. Further simulations have been performed to demonstrate the performance of the two-scale implementation. In the first example, a 3D non-symmetric notched plate with thermoelastic-viscoplastic polymer matrix reinforced by thermoelastic short glass fibers is examined under complex thermo-mechanical loading. The first example shows the effect of the loading path on the macroscopic response of the composite structure. In the second example, a cyclic loading with varying thermal boundary con-

ACCEPTED MANUSCRIPT

ditions are applied on the 3D non-symmetric notched plate consisting of a short glass fiber reinforced composite with thermoelastic-viscoplastic polymer matrix. This example illustrates the evolution of the dissipation and its influence on the temperature variations during the thermo-mechanical loading.

From a practical point of view, the proposed strategy can be used in cases of composites with strong interaction between the mechanical and thermal fields, for instance reinforced polymeric materials whose viscoplastic/viscoelastic behavior is sensitive to the temperature variations. Moreover, further investigations on local behavior can be considered, e.g., coupling of damage with the dissipation and the increase of temperature, as well as the extension of the approach towards oligocyclic fatigue analyses and life-time estimation of composite structures. It should be pointed out that such analyses are computationally time consuming and requires then certain reduction model strategies (Oliver et al., 2017).

References

Aboudi, J., 2004. Micromechanics-based thermoviscoelastic constitutive equations for rubber-like matrix composites at finite strains. International Journal of Solids and Structures 41 (20), 5611 – 5629.

Aboudi, J., Pindera, M.-J., Arnold, S.-M., 2003. Higher-order theory for periodic multiphase materials with inelastic phases. International Journal of Plasticity 19 (6), 805–847.

ACCEPTED MANUSCRIPT

ACCEPTED MANUSCRIPT

Allaire, G., 1992. Homogenization and two-scale convergence. SIAM Journal on Mathematical Analysis 23, 1482–1518.

Anagnostou, D., Chatzigeorgiou, G., Chemisky, Y., Meraghni, F., 2018. Hierarchical micromechanical modeling of the viscoelastic behavior coupled to damage in SMC and SMC-hybrid composites. Composites Part B: Engineering 151, 8–24.

Asada, T., Ohno, N., 2007. Fully implicit formulation of elastoplastic homogenization problem for two-scale analysis. International Journal of Solids and Structures 44 (22), 7261–7275.

Bensoussan, A., Lions, J.-L., Papanicolaou, G., 1978. Asymptotic methods for periodic structures.

Berthelsen, R., Denzer, R., Oppermann, P., Menzel, A., 2017. Computational homogenisation for thermoviscoplasticity: application to thermally sprayed coatings. Computational Mechanics 60, 739–766.

Bertram, A., Krawietz, A., 2012. On the introduction of thermoplasticity. Acta Mechanica 223 (10), 2257–2268.

Brenner, R., Suquet, P., 2013. Overall response of viscoelastic composites and polycrystals: exact asymptotic relations and approximate estimates. International Journal of Solids and Structures 50 (10), 1824–1838.

Chaboche, J.-L., Kanoute, P., Roos, A., 2005. On the capabilities of mean-field approaches for the description of plasticity in metal matrix composites. International Journal of Plasticity 21 (7), 1409–1434.

ACCEPTED MANUSCRIPT

Charalambakis, N., Chatzigeorgiou, G., Chemisky, Y., Meraghni, F., 2018. Mathematical homogenization of inelastic dissipative materials: a survey and recent progress. Continuum Mechanics and Thermodynamics 30, 1–51.

Chatzigeorgiou, G., Charalambakis, N., Chemisky, Y., Meraghni, F., 2016. Periodic homogenization for fully coupled thermomechanical modeling of dissipative generalized standard materials. International Journal of Plasticity 81, 18–39.

Chatzigeorgiou, G., Charalambakis, N., Chemisky, Y., Meraghni, F., 2018. Thermomechanical Behavior of Dissipative Composite Materials. ISTE Press - Elsevier, London.

Chatzigeorgiou, G., Chemisky, Y., Meraghni, F., 2015. Computational micro to macro transitions for shape memory alloy composites using periodic homogenization. Smart Materials and Structures 24 (3), 035009.

Coleman, B. D., Gurtin, M. E., 1967. Thermodynamics with Internal State Variables. The Journal of Chemical Physics 47 (2), 597–613.

Dong, H., Cui, J., Nie, Y., Yang, Z., 2017. Second-Order Two-Scale Computational Method for Nonlinear Dynamic Thermo-Mechanical Problems of Composites with Cylindrical Periodicity. Communications in Computational Physics 21 (4), 1173–1206.

Drago, A., Pindera, M.-J., 2007. Micro-macromechanical analysis of heterogeneous materials: Macroscopically homogeneous vs periodic microstructures. Composites Science and Technology 67 (6), 1243 – 1263.

ACCEPTED MANUSCRIPT

URL http://www.sciencedirect.com/science/article/pii/S0266353806000844

Ene, H. I., 1983. On linear thermoelasticity of composite materials. International Journal of Engineering Science 21 (5), 443–448.

Feyel, F., Chaboche, J.-L., 2000. Fe2 multiscale approach for modelling the elastoviscoplastic behaviour of long fibre sic/ti composite materials. Computer Methods in Applied Mechanics and Engineering 183 (3), 309 – 330.

Forest, S., 2009. Micromorphic approach for gradient elasticity, viscoplasticity, and damage. Journal of Engineering Mechanics 135, 117–131.

Germain, P., 1973. Cours de mécanique des milieux continus, Tome I: Théorie Générale. Masson, Paris.

Germain, P., 1982. Sur certaines définitions liées à l'énergie en mécanique des solides. International Journal of Engineering Science 20 (2), 245–259.

Germain, P., Nguyen, Q. S., Suquet, P., 1983. Continuum thermodynamics. Journal of Applied Mechanics 50, 1010–1020.

Hill, R., 1967. The essential structure of constitutive laws for metal composites and polycrystals. Journal of the Mechanics and Physics of Solids 15 (2), 79–95.

Khatam, H., Pindera, M.-J., 2010. Plasticity-triggered architectural effects in periodic multilayers with wavy microstructures. International Journal of Plasticity 26 (2), 273–287.

ACCEPTED MANUSCRIPT

Kouznetsova, V., Geers, M. G. D., Brekelmans, W. A. M., 2002. Multi-scale constitutive modelling of heterogeneous materials with a gradient-enhanced computational homogenization scheme. International Journal for Numerical Methods in Engineering 54 (8), 1235–1260.

Kruch, S., Chaboche, J.-L., 2011. Multi-scale analysis in elasto-viscoplasticity coupled with damage. International Journal of Plasticity 27 (12), 2026–2039.

Lemaitre, J., Chaboche, J.-L., 1990. Mechanics of solid materials. Cambridge University Press.

Li, S., 1999. On the unit cell for micromechanical analysis of fibre-reinforced composites. Proceedings of the Royal Society of London A 455 (1983), 815–838.

Li, S., 2000. General unit cells for micromechanical analyses of unidirectional composites. Composites: Part A 32, 815–826.

Meraghni, F., Desrumaux, F., Benzeggagh, M.-L., 2002. Implementation of a constitutive micromechanical model for damage analysis in glass mat reinforced composite structures. Composites Science and Technology 62 (16), 2087–2097.

Mercier, S., Molinari, A., 2009. Homogenization of elastic–viscoplastic heterogeneous materials: Self-consistent and mori-tanaka schemes. International Journal of Plasticity 25 (6), 1024–1048.

Mercier, S., Molinari, A., Berbenni, S., Berveiller, M., 2012. Comparison of different homogenization approaches for elastic–viscoplastic materials.

ACCEPTED MANUSCRIPT

Modelling and Simulation in Materials Science and Engineering 20 (2), 024004.

Murat, F., Tartar, L., 1997. H-convergence, in Topics in the mathematical modelling of composite materials. In: Cherkaev, A., Kohn, R. V. (Eds.), Progress in Nonlinear Differential Equations and their Applications. Vol. 31. Birkhäuser, Boston, pp. 21–43.

Nezamabadi, S., Zahrouni, H., Yvonnet, J., Potier-Ferry, M., 2010. A multiscale finite element approach for buckling analysis of elastoplastic long fiber composites. International Journal for Multiscale Computational Engineering 8, 287–301.

Oliver, J., Caicedo, M., Huespe, A., Hernández, J., Roubin, E., 2017. Reduced order modeling strategies for computational multiscale fracture. Computer Methods in Applied Mechanics and Engineering 313, 560 – 595. URL http://www.sciencedirect.com/science/article/pii/S0045782516303322

Özdemir, I., Brekelmans, W. A. M., Geers, M. G. D., 2008a. Computational homogenization for heat conduction in heterogeneous solids. International Journal for Numerical Methods in Engineering 73 (2), 185–204.

Özdemir, I., Brekelmans, W. A. M., Geers, M. G. D., 2008b. Fe2 computational homogenization for the thermo-mechanical analysis of heterogeneous solids. Computer Methods in Applied Mechanics and Engineering 198 (3), 602–613.

ACCEPTED MANUSCRIPT

Ponte-Castañeda, P., 1991. The effective mechanical properties of nonlinear isotropic composites. Journal of the Mechanics and Physics of Solids 39 (1), 45–71.

Praud, F., Chatzigeorgiou, G., Bikard, J., Meraghni, F., 2017. Phenomenological multi-mechanisms constitutive modelling for thermoplastic polymers, implicit implementation and experimental validation. Mechanics of Materials 114, 9–29.

Sanchez-Palencia, E., 1978. Non-homogeneous media and vibration theory. In: Lecture Notes in Physics 127. Springer-Verlag, Berlin.

Sengupta, A., Papadopoulos, P., Taylor, R. L., 2012. A multiscale finite element method for modeling fully coupled thermomechanical problems in solids. International Journal for Numerical Methods in Engineering 91, 1386–1405.

Shuguang, L., Anchana, W., 2004. Unit cells for micromechanical analyses of particle-reinforced composites. Mechanics of Materials 36 (7), 543–572.

Suquet, P., 1983. Analyse limite et homogeneisation. Comptes Rendus de l'Académie des Sciences, Paris II 295, 1355–1358.

Suquet, P. M., 1987. Elements of homogenization for inelastic solid mechanics. In: Lecture Notes in Physics. Vol. 272. Springer, Berlin, pp. 193–278.

Temizer, I., 2012. On the asymptotic expansion treatment of two-scale finite thermoelasticity. International Journal of Engineering Science 53, 74–84.

ACCEPTED MANUSCRIPT

Terada, K., Kikuchi, N., 2001. A class of general algorithms for multi-scale analyses of heterogeneous media. Computer Methods in Applied Mechanics and Engineering 190 (40), 5427–5464.

Tikarrouchine, E., Chatzigeorgiou, G., Praud, F., Piotrowski, P., Chemisky, Y., Meraghni, F., 2018. Three-dimensional fe2 method for the simulation of non-linear, rate-dependent response of composite structures. Composite Structures 193, 165–179.

Xu, R., Bouby, C., Zahrouni, H., Ben Zineb, T., Hu, H., Potier-Ferry, M., 2018. 3d modeling of shape memory alloy fiber reinforced composites by multiscale finite element method. Composite Structures 200, 408 – 419.

Yu, Q., Fish, J., 2002. Multiscale asymptotic homogenization for multiphysics problems with multiple spatial and temporal scales: a coupled thermo-viscoelastic example problem. International Journal of Solids and Structures 39 (26), 6429–6452.

ACCEPTED MANUSCRIPT